Progress in Oceanography 214 (2023) 102982

Contents lists available at ScienceDirect

Progress in Oceanography

journal homepage: www.elsevier.com/locate/pocean

Iron and silicic acid addition effects on early spring macronutrient drawdown and biogenic silica production of Patagonia estuarine waters

Rodrigo Torres [a,b,*], Brian Reid [a], Gemita Pizarro [c], Máximo Frangópulos [b,d,e,f], Emilio Alarcón [a,b], Magdalena Márquez [g], Francisco Díaz-Rosas [i], Eduardo Menschel [a,b], Humberto E. González [b,h], Paulo Moreno-Meynard [a,j], Paulina Montero [a,m], Hernán Pacheco [c], Marco Pinto-Torres [b,n,o], Cesar Alarcón [c], Rodrigo Ibañez [k], Jon Hawkings [l]

[a] Centro de Investigación en Ecosistemas de la Patagonia (CIEP), Coyhaique, Chile
[b] Centro de Investigación: Dinámica de Ecosistemas Marinos de Altas Latitudes (FONDAP-IDEAL), Valdivia y Punta Arenas, Chile
[c] Instituto de Fomento Pesquero (IFOP), Punta Arenas, Chile
[d] Centro de Investigación GAIA Antártica (CIGA), Universidad de Magallanes, Punta Arenas, Chile
[e] Cape Horn International Center (CHIC), Punta Arenas, Chile
[f] Millenium Institute "Biodiversity of Antarctic and Subantarctic Ecosystems" (BASE), Santiago, Chile
[g] Graduate program, Universidad Austral de Chile, Chile
[h] Instituto de Ciencias Marinas y Limnológicas, Universidad Austral de Chile, Valdivia, Chile
[i] Facultad de Ciencias Biológicas, Departamento de Ecología, Pontificia Universidad Católica de Chile, Santiago, Chile
[j] Graduate program, Department of Earth, Environmental and Life Sciences, University of Genoa, Genoa, Italy
[k] Graduate program, Departamento de Geofísica, Universidad de Concepción, Concepción, Chile
[l] Department of Earth and Environmental Science, University of Pennsylvania, Philadelphia, PA, USA
[m] Centro de Investigación Oceanográfica COPAS COASTAL, Universidad de Concepción, Chile
[n] Services and Consulting HABs SpA, Punta Arenas, Chile
[o] Programa de Doctorado en Ciencias de la Acuicultura, Universidad Austral de Chile, Puerto Montt, Chile

A B S T R A C T

The Patagonia archipelago interior sea (PAIS) of southern Chile is one of the largest fjord systems on earth. These coastal waters include remote and virtually pristine areas where extreme rainfall/runoff and glacial meltwaters intensify the land–ocean interaction impinging on the biological, physical, and chemical characteristics of oceanic subantarctic Surface Water (SAASW) that flood the archipelago basins. The SAASW mix with silicon- and iron-replete continental water and diatom growth would occur concomitantly with a rapid drawdown of SAASW macronutrients. Consequently, phytoplankton metabolism (e.g. macronutrient utilization for primary productivity) in estuaries of southern Patagonian has been previously assumed independent of iron availability (i.e. iron-replete conditions). Experimental results shown here suggest that the nitrate and phosphate drawdown in low salinity (29) water can be enhanced by a 5 nM dissolved iron enrichment (by 13% and 28%, respectively) during the developing phase of a diatom bloom. The simultaneous enrichment in iron (5 nM) and silicic acid (5 μM) in these estuarine waters resulted in a similar macronutrient uptake enhancement, a 119% increment of the production of biogenic silica and a 2-fold rise in the abundance of *Pseudo-nitzschia spp* (a diatom capable to produce the neurotoxin domoic acid). We suggest that natural freshwater pulses of allochthonous bioavailable forms of iron and silicon to inner waters of the Patagonia archipelago during the onset of the productive season play a potentially significant role modulating macronutrient dynamics (input vs utilization) and influencing coastal phytoplankton assemblages.

1. Introduction

Iron (Fe) is an essential micronutrient for marine phytoplankton, and its availability limits primary production in 30–50 % of the surface ocean (Boyd et al., 2007; de Baar et al., 2005; Sunda and Huntsman, 2011). Fe plays a key role in multiple microbial physiological pathways (Raven et al., 1999) including the capacity to utilize macronutrients (e.g. NO_3^-) and resources (e.g. light) (Falkowski & Raven, 1997). Iron limitation in the ocean is primarily associated with poor solubility of thermodynamically stable Fe(III) chemical species in well-oxygenated surface waters and distance from continental Fe sources (de Baar et al., 1999; Liu & Millero, 2002; Martin & Fitzwater, 1988). Coastal waters are proximal to Fe sources and are often characterized by elevated levels of iron, particularly in the form of particles and colloids

* Corresponding author.
E-mail address: rtorres@ciep.cl (R. Torres).

https://doi.org/10.1016/j.pocean.2023.102982

Available online 20 March 2023

(Batchelli et al., 2010; Fujii et al., 2008; Gobler et al., 2002; Kunde et al., 2019; Nishioka et al., 2001; Raiswell and Canfield, 2012; von der Heyden and Roychoudhury, 2015; Raiswell et al., 2006). The dissolved iron concentration is controlled by several processes and factors (Croot & Heller, 2012), including the availability of organic Fe-chelators that raise the solubility limit (Kuma et al., 1996, 1998; Liu and Millero, 2002) and the scavenging of iron on to particles (Seo et al., 2022; Tagliabue et al., 2019).

Low concentrations of trace-nutrients (e.g. Fe) and other resources (e.g. silicic acid, light) in macronutrient-rich waters promote the proliferation of smaller organisms and functional groups with adaptations for coping with environmental stressors (e.g. larger surface/area ratio, low or no Si requirement, vertical mobility, mixotrophic capacity (Caron et al., 2017; Finkel et al., 2010; Lewis, 1976). However, both smaller sized phytoplankton, as well as other functional groups, struggle to outcompete diatoms under resource replete conditions. The success of coastal diatoms as dominant phytoplankton groups in dynamic and nutrient-rich coastal waters partially rely on their capacity to acclimatize to rapid fluctuations in light availability and to rapidly use available macronutrients (e.g. NO_3^- and PO_4^{3-}). The ability to rapidly utilize macronutrients requires Fe-rich photosynthetic architecture (Strzepek & Harrison, 2004) and Fe-based enzymatic pathways for the reduction of thermodynamically stable forms of inorganic nitrogen (Schoffman et al., 2016). Diatoms have likely evolved to cope with Fe limitation (Lampe et al., 2018) implying that more recently evolved branches of diatoms (i.e. Coscinodiscophytina, Coscinodiscophyceae; Medlin & Kaczmarska, 2004) could be less sensitive to iron levels of the modern ocean. Genes for iron storage proteins such as Ferritin have been discovered in diatoms (Marchetti et al., 2009). It has been shown that Ferritin-containing pennate diatom *Pseudo-nitzschia granii*, native to iron-limited waters of the Northeast Pacific Ocean, exhibited an exceptionally large luxury iron storage capacity and increased ferritin gene expression at high iron concentrations (Cohen et al., 2018). However, in general, no systematic differences among Ferritin-containing and non-Ferritin containing diatom lineages has been observed related to their ability to store iron in excess of that needed to support maximum growth rates (Cohen et al., 2018). It has been suggested that Ferritin may serve multiple functional roles that are independent of diatom phylogeny (Cohen et al., 2018).

Diatom growth requires silicic acid (DSi), but silicification of diatom frustules is highly plastic, allowing them to grow in a wide range of environments. Hence diatoms can significantly reduce their silicification levels under silicon-limited conditions (Ragueneau et al., 2000), however DSi concentration < 2 μM often preclude diatoms to dominate the phytoplankton ensemble (Egge & Aksnes, 1992). Diatoms stressed by macro or micronutrients shortage (e.g. Fe, N) can continue silicification depending on the availability of DSi. Indeed, iron limitation in macronutrient and DSi rich waters induce high DSi/N uptake ratios (Hutchins & Bruland, 1998; Takeda, 1998), potentially leading to High Nutrient Low Silicate Low Chlorophyll (HNLSiLC) conditions. Although iron limitation effect on DSi/N uptake rates in diatoms can be fully reverted after iron enrichment (Brzezinski et al., 2002; Franck et al., 2000, 2003), the DSi deficient seawater relative to N will remain unless an allochthonous Si input occurs. Iron stimulated diatom division rate in low DSi but N and P-rich waters could result in thin frustules due the dependency in the extent of silicification on the growth rate (Martin-Jézéquel et al., 2000).

N and Si metabolism in diatoms are not closely tied since cellular energy for silicification and transport comes from aerobic respiration without any direct involvement of photosynthetic energy (Martin-Jézéquel et al., 2000). Therefore, it has been proposed that when both Si and Fe are depleted, Si uptake is limited by silicic acid concentration while N uptake and photosynthesis are limited by Fe (Ragueneau et al., 2000). The degree of silicification may in turn play a role in the diatom prey-predator dynamics, frustules recycling times, cell density and therefore with the potential to modulate the channeling of diatom biomass energy through both the water column and the trophic web (Assmy et al., 2013; Grønning and Kiørboe, 2020; Kemp et al., 2000; Ryderheim et al., 2022; Smetacek, 1998; Smetacek et al., 2012). While the inputs of bioavailable Fe to nitrate rich waters could be critical in setting the timing and intensity of new productivity during the productive season of high latitude ecosystems, inputs of bioavailable Si may be pivotal in the fate of this new productivity (Martin et al., 2013). Diatom standing stock in surface waters can be controlled by mortality (e.g. grazing (Steinberg & Landry, 2017), parasitism (Tillmann et al., 1999)) and the formation of rapidly sinking aggregates (Logan et al., 1995; Mopper et al., 1995).

Bottle-incubation experiments using Subantarctic Front water at Crozet basin (Sedwick et al., 2002) showed that soon after (<4.5 days) adding iron a macronutrient drawdown increased relative controls. Greater abundance of pennate diatom and biogenic silica (bSi) were also observed in bottles that were amended with both Fe and DSi, relative to controls and bottles that were amended exclusively with Fe (Hutchins et al., 2001; Sedwick et al., 2002). Similar experiments conducted in equatorial Pacific HNLCLSi surface waters demonstrated that the simultaneous addition of Fe and DSi enhanced rates of diatom organic matter accumulation and cell division (Marchetti et al., 2010). Larger diatom standing stock after the addition of both DSi and Fe could be attributed to large diatom growth rates and/or lower diatom mortality rates compared to controls.

Micro-zooplankton grazing is considered one of the largest loss factors of marine primary production (Calbet & Landry, 2004; Steinberg & Landry, 2017). Heterotrophic dinoflagellates can comprise 60–80% of microplankton grazer biomass during spring blooms at high latitudes (Menden-Deuer et al., 2018). In subantarctic waters dinoflagellates of the genus *Gymnodinium* and *Gyrodinium* have been reported to feed and grow on diatom blooms (Saito et al., 2006). Grazer activity is significantly modulated by the characteristic of the prey (e.g. size, shape, silicification degree, physiological state (Assmy et al., 2013; Liu et al., 2016; Lürling, 2021)) which in turn can be a function of the availability of nutrients and silicic acid, among other factors.

The natural enrichment of Fe and DSi in macronutrient-rich eastern Pacific subantarctic waters could be a key process driving the shift in phytoplankton assemblage from flagellates (e.g. *Prymnesiophytes*) dominating in open eastern Pacific subantarctic waters (Bouman et al., 2012; de Baar et al., 1999) to large diatoms dominating in the inner waters of PAIS during the productive growing season (Iriarte et al., 2001). The orographic effect of the Patagonian Andes intercepting the moist Westerlies (Smith & Evans, 2007) results in a major supply of terrestrial waters and associated solutes into the coastal ocean. Large volume of precipitation, run-off and continental ice melt result in a buoyant surface layer likely enriched in allochthonous "continental" nutrients (e.g. silicon and iron e.g. (Hopwood et al., 2019; Torres et al., 2014; Pryer et al., 2020)) which are scarce in the subantarctic open waters (Sarmiento et al., 2004; Torres et al., 2014) that flow into the archipelago. However, the internal cycling of bioavailable forms iron in the water column (Tagliabue et al., 2019), the complex interaction between continent-ocean–atmosphere, and the estuarine metabolism (Bianchi, 2007; Bianchi et al., 2020) are expected to drive high spatio-temporal variability of the concentration of terrestrially derived bioactive elements (e.g. silicon and iron).

High nutrient low chlorophyll (HNLC) concentrations in the euphotic layer during austral spring has been reported in the southern western portion of the Patagonian archipelago (Iriarte et al., 2018). While the observation of "coastal HNLC'' conditions during austral spring has been attributed to light (low stratification) and DSi deficit waters because of oceanic SAASW intrusion into the archipelago, events of high biological productivity and drastic drops in surface seawater pCO_2 are often associated to stratification forced primarily from freshwater discharge from the continent. Indeed, along Patagonia, surface waters of salinity lower than 28 are typically undersaturated in pCO_2 during the productive season (Torres et al., 2011b). Fe has been shown to be the limiting

nutrient in the productive continental shelves surrounding the Antarctic continent; however, no attempt to assess the levels of dissolved Fe or test its effects on phytoplankton has been reported for PAIS. The bioavailability of Fe in PAIS has been assumed to be replete for phytoplankton needs due the many and varied potential sources of Fe (e.g. large amount surface runoff (Dávila et al., 2002) and glacial meltwater inputs (Chen et al., 2007; Glasser et al., 2011; Hopwood et al., 2019; Willis et al., 2012). However, removal of dissolved iron at low salinities in estuaries can be significant due to flocculation, aggregation, and scavenging from the euphotic zone (Boyle et al., 1977; Hopwood et al., 2016; Schroth et al., 2014; Sholkovitz, 1976; Sholkovitz et al., 1978; Yeats & Bewers, 1976). Processes of bioavailable Fe removal could lead to suboptimal conditions for blooming phytoplankton in fjord waters (Öztürk et al., 2002). Currently, comprehensive datasets and integrated analysis of trace metals, nutrients and phytoplankton characteristics in the productive dynamic of this austral ecosystem are lacking.

We report an on-deck nutrient addition bottle incubation experiment as an initial attempt to explore the response of phytoplankton communities in southern PAIS waters to Fe and Fe + DSi amendments. We test the microbial consortia's capacity to use macronutrients (nitrate, phosphate, silicate, carbon) and phytoplankton (diatom and dinoflagellates) abundance, composition, allocation of photosynthetic pigments in different size ranges, cellular domoic acid (DA) production and biogenic silica concentration. Additionally, we describe the spatial variability of the majority of variables mentioned above for a latitudinal transect along the southern portion of the PAIS (53.5°S-50.5°S) with a spatial resolution of < 15 km during austral spring. The discussion of survey results will explore the effect of continental freshwater discharge and associated solutes on the spatial–temporal variability of diatom blooms in southern Patagonia.

2. Methods

2.1. Study area

Hyper humid subantarctic fjords and continental reservoirs of freshwater (including ice fields and peatlands) result in high levels of freshwater discharge year-round, particularly during the warm summer period associated with snow and glacier melting as is observed in the largest hydrographic basin of the study area (Rio Serrano basin, Fig. 1).

Freshwater discharge varied spatially depending on hydrographic basin configuration, latitudinal and longitudinal gradients in precipitation associated with westerlies, with maximum levels (up to 7–10 m y^{-1}) at the western boundary of the archipelago where hydrographic basins are small (e.g. near 50°S) contrasting with large hydrographic basin at the continental side. The continental inputs include different freshwater discharge sources (glacier runoff and non-glacier runoff fed by direct precipitation) that flow into coastal waters, likely influencing the dissolved and particulate material loads of freshwaters (Pryer et al., 2020; Pryer et al., 2019).

The transect of marine interior fjord waters starts in the Magellan Strait, running from Peninsula Brunswick near the mouth of Otway sound (Sta. 1; 53.7S) to the mouth of Xaultegua Gulf (Sta. 7; 53.1° S), where the transect is interrupted by western ocean exposure, resuming in interior waters near Isla Renourd (Sta. 8; 52.6° S) and continuing until Madre de Dios Archipelago (Sta. 29; 50.5 °S). The transect is therefore characterized by constrained inland marine waters in close contact with innumerable small to medium point sources of continental runoff, areas of concentrated high-volume runoff where interior canals connect with the large Rio Serrano basin (Stations 12–13, near the western mouth of Union Channel), and areas of glacial input from the Darwin Range (Stations 1–2) and the Southern Patagonia Icefields (Stations 17–22). In

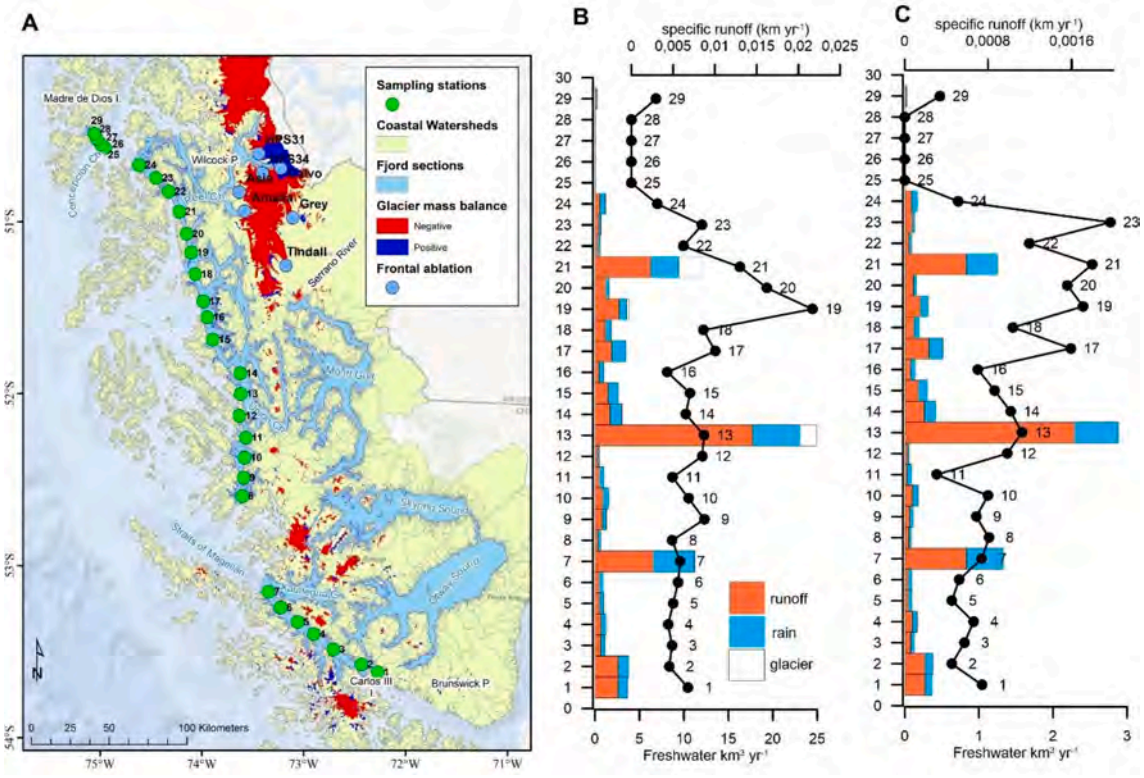

Fig. 1. Surface water sampling stations and estimation of freshwater inputs linked to transect stations. Left panel shows stations along the coastal transect of fjords and channels spanning 3°. Also shown are coastal watersheds providing runoff from adjacent terrestrial sources, together with glacial inputs indicated by areas of receding glaciers, and net changes in ice field thickness. Central panel summarized mean annual freshwater volume input near sampling stations and respective sources along the transect, based on calculation shown in **Supl. Table A1**. Right panel summarized freshwater input near the stations during August and September 2017 and respective sources along the transect, based on calculation shown in **Supl.Mat A**.

addition to runoff generated from continental basins and glacial meltwater, direct precipitation is expected to contribute a significant percentage of dilute freshwater input along the transect, which is characterized by a precipitation gradient ranging from 2.000 to 7.000 mm y^{-1}. Surface lithology along this transect is diverse (Torres et al., 2014), as is vegetation cover (Luebert & Pliscoff, 2006) and potentials soils (virtually uncharacterized, but likely ranging from volcanic Andosols, Entisols in recently deglaciated areas, and abundant Histosols corresponding with extensive wetlands). The corresponding quality of freshwater inputs, in terms of nutrients and other solutes is also expected to be diverse but remains poorly unknown. Partitioning of freshwater inputs is generalized here (Fig. 1b, 1c) as direct precipitation (trace solutes), glacial runoff (high suspended load and low nutrient), and land-surface runoff (diverse and variable solute and suspended load). The experimental location and surface water grab samples which constitute the experimental matrix were between stations 25 and 29 (Fig. 1, Concepción Channel), at the end of the fjord transect near the Madre de Dios Archipelago, representing transitions in surface runoff lithology from crystaline/granitic to sedimentary limestone, strong climatic gradient, and geographic transition from inner to outer fjords, with corresponding gradients in salinity and terrestrial subsidy (described in Torres et al., (2020)).

2.2. Underway sampling

Underway sampling of surface waters from 53.5°S to 50.5°S (Fig. 1) was carried out from 22 to 23 September 2017. Surface water was collected at ~ 1 m depth and ~ 3 m off the side of the vessel using a lab-made, metal free, tow "fish'' connected through polyethylene tubes with two non-metallic ARO™ air operated diaphragm pumps. All surfaces that came into contact with the sample were acid cleaned. One sampling line outlet, was located inside a small (1 m^2) flow laminar bench to allow clean sampling (used exclusively to trace metal work), and the other sampling line outlet was connected to a small CTD (Idronaut 304) and used to collect discrete samples for determining pH, A_T, nitrate, phosphate, silicic acid (DSi), biogenic silica and size fractionated chlorophyll *a* (chl a). This underway system was used to collect 29 discrete seawater surface samples (Stations 1–29, Fig. 1a,b) at an approximate rate of one sample per hour while steaming (8–14 km h^{-1}) along the track shown in Fig. 1a.

2.3. Incubation water

Unfiltered surface seawater for bottle incubation experiments was collected using the tow fish systems described above. Twelve acid cleaned (soaked in 10% trace metal grade HCl for 3 months), and carefully rinsed with 18.2 MΩ cm^{-1} milli-Q water within a laminar flow bench. 25 L polycarbonate carboys (Nalgene) were filled with surface seawater while steaming at low speed (<8 km h^{-1}) across Concepcion channel (CC), from St. 25 to St. 27 (Fig. 1). The carboys correspond to four groups (G1 to G4) of three 25 L incubations carboys (control, +Fe, and + Fe + Si; i.e. 12 carboys in total). Each group was filled virtually simultaneously immediately before station 25, between stations 25–26, 26–27, and immediately before station 27. Iron enrichments were spikes of an aqueous solution of $FeCl_3$ to a final concentration of 5 nM. Similarly, Fe and Si enrichments to a final solution of 5 nM (Fe) and 5 μM (Si) were achieved by the addition of aliquots of aqueous solutions of $FeCl_3$ and Na_2SiO_3. Environmental DSi variability ranged between 3 and 9 μM therefore it is likely that initial concentration of DSi in the Si enrichment treatments (i.e. + Fe + DSi) lay between 44% and 133% the initial DSi concentration in control and + Fe treatment (see discussion Section 4). We measured total dissolved iron (dFe, see method Section 2.7) at the end of each experiment, and it ranged from 4.9 nM to 11.4 nM. The average net increment in dFe in iron enriched carboys (i.e. + Fe and + Fe + Si) relative to controls was ca. 1 nM (see Section 3.2; Fig. 3).

The 12 carboys were incubated on deck for three days (the daylength was ~ 12 h) and immersed in an intermittently surface seawater running water bath to keep them near the ambient sea surface water temperature (ca. 8 °C, see Fig. 2h). Immediately after the incubation period, pH was measured and subsamples were collected for size-fractionated chlorophyll *a*, macronutrients, biogenic silica, domoic acid, phytoplankton abundance and SEM identification, total alkalinity, and salinity.

2.4. Salinity and carbonate system parameters

Discrete samples collected along the transect were analyzed for salinity with a salinometer (YSI Model Pro30; calibrated with IAPSO standard seawater) at a constant temperature of 25.0 °C. Total alkalinity (A_T) was determined using an automatic potentiometric titration system (Haraldsson et al., 1997). A_T accuracy was verified with certified reference material (CRM) supplied by Andrew Dickson (Scripps Institution of Oceanography). Based on the analysis of blind A_T samples during the "2017 Inter-laboratory Comparison of CO_2 Measurements" (coordinated. Emily Bockmon and Andrew Dickson, unpublished data) we estimate deviations of approximately 0.1% from the reference value (uncertainties ca. 2 μmol kg^{-1}). Surface seawater pH was measured in discrete samples immediately after collection, at a constant temperature (25.0 °C), following (DOE, 1994) using a Metrohm pH meter (model 780) and a glass-fixed ground-joint diaphragm electrode with an integrated platinum resistance thermometer (model Aquatrode Plus, Metrohm) calibrated every 12 h with Tris buffer in synthetic seawater. Accuracy was previously verified using a certified Tris buffer supplied by Andrew Dickson Laboratory (Scripps Institution of Oceanography), and the overall uncertainty in the measured pH values was estimated by Torres et al. [1999] as 0.006 pH units for marine surface waters. A previous at-sea comparison between pH measured by spectrophotometric (DOE, 1994) and pH measured by the potentiometric method described above, showed absolute mean differences of 0.01 pH units in the salinity range from 22 to 27 (E. Alarcón, unpublished data). Carbonate system speciation and the seawater saturation state with respect to calcium carbonate (Omega) were determined using CO2SYS software (Lewis & Wallace, 1998) set with K_1 and K_2 constants (Dickson & Millero, 1987) derived from a refit of Mehrbach solubility data (Mehrbach, Culberson, Hawley & Pytkowicz, 1973), using measured values of pH, A_T, temperature, salinity, silicic acid, and phosphate. Overall uncertainties in the calculated pCO_2 and C_T, including those derived from uncertainties in carbonate system measurements and uncertainties in constants (K_0, K_1, and K_3), were previously estimated to be approximately 9 μatm and 9 μmol kg^{-1}, respectively (Torres et al., 1999).

2.5. Nutrients, fractionated chlorophyll a and biogenic Si

Nitrate, nitrite, phosphate and silicic acid (DSi) were analyzed colorimetrically following (Strickland & Parsons, 1968) manual method. The standard solutions were made from salts of KNO_3 (Riedel-de Haën Lot 6167A), $NaNO_2$ (Riedel-de Haën Lot 51010) and KH_2PO_4 (Riedel-de Haën Lot 53550), in the case of silicic acid, a Merck™ silicon standard solution (traceable to NIST Standard Reference Material) was used. Although no replicates or other assessment of precision was performed during the analysis of the samples, the attainable precision for the used methods is likely < 6% (Grasshoff et al., 1999). We use Whatman GF/F 0.7 μm glass microfiber filters, 0.45 μm and 2 μm polycarbonate membranes, in combination with 20 μm and 200 μm mesh nets to fractionate phytoplankton in three size fractions: 0.45–2 μm, 2–20 μm, 0.7–200 μm. The 0.45, 0.7 and 2 μm filters were kept in liquid nitrogen, until pigments were extract in 90% acetone solution to be analyzed for chlorophyll *a* (chl a) using a Trilogy Turner Designs fluorometer previously calibrated with a *Anacystis nidulans* chl a standard (Strickland & Parsons, 1968). Each individual chla measurement was done without replicates. Size fractionated chl a was classified as pico-chl a (0.45–2 μm), nano-chl a (2–20 μm) and total-chl a (0.7–200 μm). The difference between the total chla and the sum of pico and nano chl a and was assumed equal to

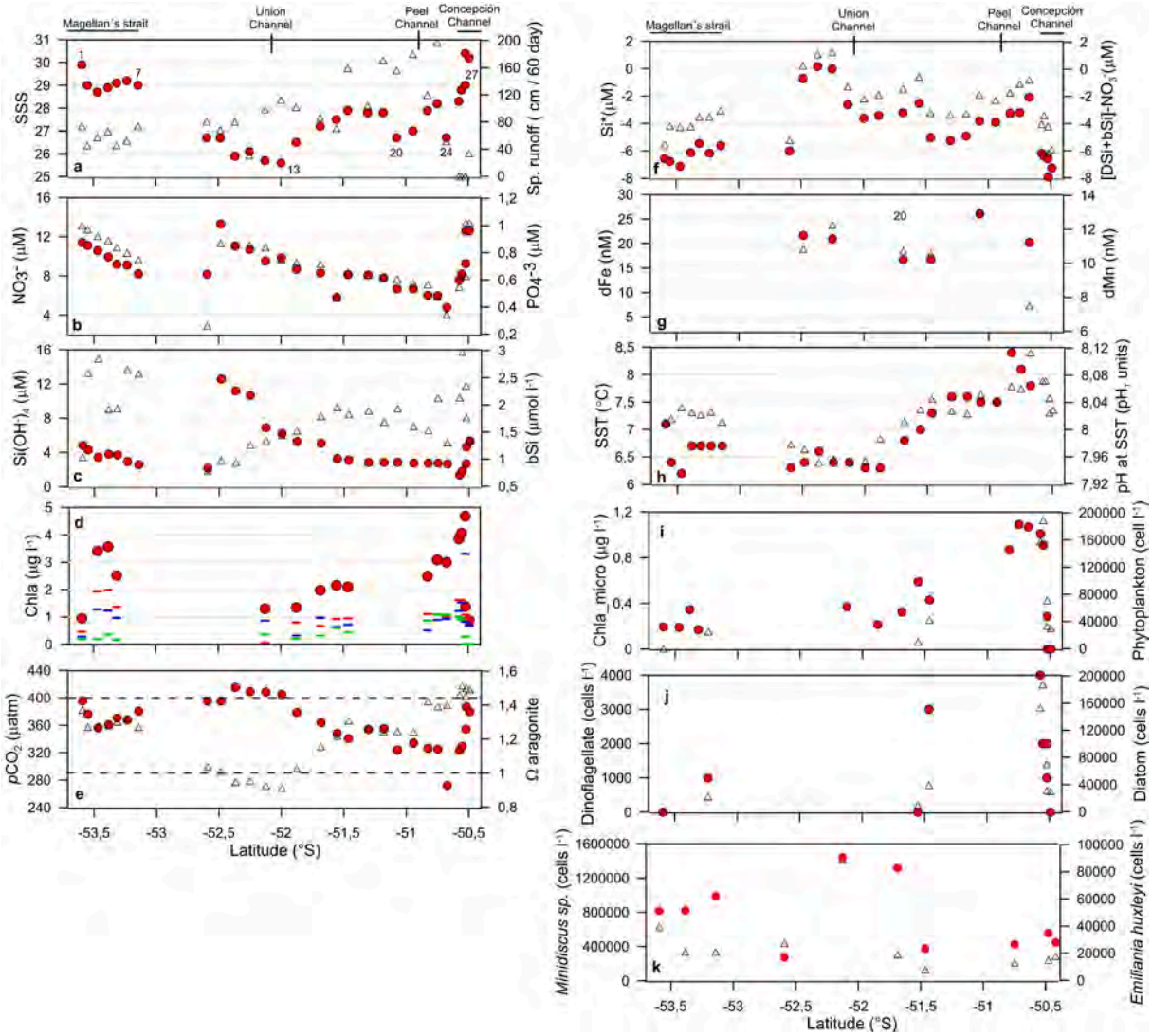

Fig. 2. Surface water properties and freshwater inputs along a transect during austral spring 2017. Dots and triangles correspond to the left and right axis respectively. (a) Sea Surface Salinity (SSS) and 60 days mean specific runoff (cm / 60 days) corresponding to august and september 2017 based on Fig. 1c, (b) nitrate (NO_3^-) and phosphate (PO_4^{3-}), (c) dissolved silicate (DSi) and biogenic silicate (bSi), (d) Chlorophyll *a* (chl a) allocated in the pico, nano and micro size fraction are depicted by the red, blue and green horizontal line, respectively. The summa of all three fractions (total_chl a) is depicted by red dots. (e) Carbon dioxide partial pressure (pCO_2) and Omega Aragonite ($\Omega_{aragonite}$), atmospheric pCO_2 and calcium carbonate saturation with respect to seawater is depicted by upper and lower segmented lines, respectively. Surface water properties and freshwater inputs along a transect during austral spring 2017. Dots and triangles correspond to the left and right axis, respectively. (f) Silica star (Si*) and the difference between total silicate and nitrate ([DSi + bSi]–NO_3^-). (g) dissolved iron (dFe) and dissolved manganese (dMn). (h) Sea Surface Temperature (SST) and Total-scale pH at in situ temperature. (i) chlorophyll *a* allocated in the micro size fraction (micro-chl a) and micro-phytoplankton abundance. (j) Dinoflagellate and diatom abundance. (k) Abundances of Minidiscus spp. and Emiliania huxleyi estimated by SEM. Abundance estimations of E. huxleyi were taken from Díaz et al. (2021).

micro-chl a. This calculated micro-chl a (20–200 µm) value, however, could be slightly underestimated since total-chl a do not consider the fraction from 0.45 to 0.7 µm size as the pico-chl a fraction do. Indeed, in some stations calculated micro-chl a was slightly negative, in that case they were assumed equal to zero.

Biogenic silicate (bSi) of seston larger 2 µm (retained on 2 µm pore polycarbonate membrane) of one liter of sample was estimated from the digestion of particles in a 85 °C Na_2CO_3 0.5 % solution for 2 h (DeMaster, 2002). We assumed that although digestion could dissolve some lithogenic silicate (Ragueneau et al., 2005; Ragueneau and Tréguer, 1994), its effect would be minimal due the exclusion of clay (lithogenic silicate particles < 2 µm). Additionally, any relative effect would be canceled when net bSi production is calculated from the same seawater batch incubation.

2.6. Domoic acid

Samples for domoic acid (DA) were processed by vacuum filtration of 1 L seawater through a muffled 0.7 µm Whatman GF/F filter and stored in liquid nitrogen before analysis at the Marine Toxins Laboratory, University of Chile (labtox.cl). At the laboratory the individual filters were transferred to a 100% methanol solution by homogenizing the filter in 1 mL of solvent. The homogenized solution was centrifuged (14,000 rpm × 10 min), filtered through a 0.22 µm PVDF Millipore Millex-GV, and dried under nitrogen gas. The dried extract was resuspended and measured via liquid chromatography–tandem mass spectroscopy (LC-MS/MS) with a detection limit of ca. 0.025 µg DA/ml (López-Rivera et al., 2005).

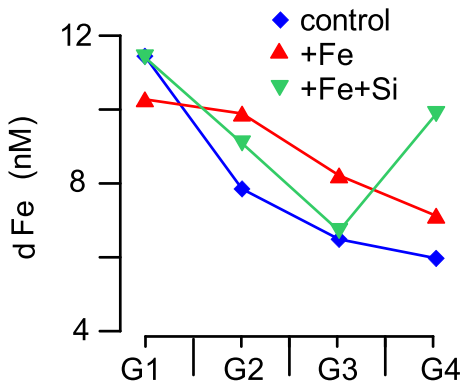

Fig. 3. Dissolved iron at t = 3 days in control carboys (blue), enriched in Fe (red) and enriched in both Fe and Si (green). The values of Fig. 3 can be inspected in supplementary material D.

2.7. Phytoplankton

2.7.1. Phytoplankton abundance determined by optic microscopy.

Samples for phytoplankton cell counts were preserved in Lugoĺs solution. For samples along the transect (Fig. 1) a 50-mL sub-sample was placed in a sedimentation chamber and allowed to settle for 24 h (Utermohl, 1958) prior to identification under an inverted microscope (Carl Zeiss, Axio Observer A.1). Phytoplankton counting was done without replicates. For experimental samples, phytoplankton abundance was determined similarly (Utermohl, 1958) at the IFOP phytoplankton laboratory (IFOP-Punta Arenas).

2.7.2. Phytoplankton abundance determined by Scanning Electron Microscopy.

Scanning Electron Microscopy (SEM) imagery (Díaz-Rosas et al., 2021) was used to facilitate phytoplankton identification, diatom volume and estimation of the abundance of *Minidiscus* spp. with apical axis smaller than 3.5 μm (see an example SEM imagery in Supplementary Material B). Intact frustules (single or in aggregates) were counted in 36 SEM images per sample, covering 1.8 mm^2 of the filter area corresponding to 1.5 mL of water analyzed. The *Minidiscus* spp. (Rivera and Koch, 1984) abundances were calculated using the same equation for coccolithophores given in Díaz-Rosas et al. (2021)

2.7.3. Diatom biovolume

Several geometric shapes were selected for determining biovolume of diatoms according mainly to (Naz et al., 2013; Olenina et al., 2006), and the website https://nordicmicroalgae.org. The linear dimensions were measured digitally, through scanning electronic photomicrographs using the Photoshop™ software. The volume of each cell was measured and computed in an excel worksheet by applying average dimensions for each species to its most closely geometrical shape (cylinder, sphere, ellipsoid, cone, etc.). For each treatment, at least 30 randomly selected cells for each species were measured, and in the case of rare species, they were measured as they occurred. The mean biovolume was calculated from the mean value individual cell biovolumes.

2.7.4. Diatom total volume

Total diatom volume was defined as the sum of total volume of each taxa, where the total volume of a particular taxa was equal to an average diatom-taxon biovolume multiplied by diatom-taxa abundance. Therefore, the relative differences in total biovolume of diatoms reported here (comparison between treatments) indicates a change on the diatom assemblage size structure. We assume that biovolume errors are primarily systematic (associated with the simplification of diatom shape to perform the volume calculations, see section 2.6.3) which tend to cancel out when analyzed in relative terms, and the non-systematic errors (which is a function primarily dependent on the number of measured individuals) are minimized in the most abundant taxa (were the biometric measurements were carried out in 30 organisms per specie, see section 2.6.3). However, we did not attempt to estimate the error of our estimation of total diatom biovolume (since diatom-taxa abundance was done without replicates) and therefore these estimates should be viewed with caution and analyzed in relative terms.

2.7.5. Mean diatom cell volume

Defined as diatom total volume/ diatom abundance ratio. Mean diatom cell volume is therefore exclusively driven by changes in the size structure of the diatom community.

2.8. Dissolved iron measurements

Seawater samples were filtered through an acid cleaned 0.45 μm capsule filter (Whatman PolyCap GW) and subsequently through a 0.02 μm Anotop 25 syringe filter (pre-cleaned with 0.02 M ultra trace metal grade HCl as per (Hawkings et al., 2020)) inside a flow laminar bench into acid cleaned LDPE bottles (cleaned as per GEOTRACES protocols; Cutter et al., (2017)). Samples were acidified with hydrochloric acid to pH ~ 2 in a Class 100 clean room bench and let stand for a month before analysis for Fe, Mn and other metals (not shown here) after preconcentration and matrix removal using an ESI seaFAST pico system. Isotope dilution inductively coupled plasma mass spectrometry (on a sector field inductively coupled plasma mass spectrometer Thermo Element 2) was used to determine Fe concentrations as described in Forsch et al. (2021). Accuracy and precision for Fe were ± 3 %, as determined by repeat measurements of an in-house low Fe seawater reference standard. We use the naming convention of Raiswell et al., 2018 for < 0.45 μm and < 0.02 μm filtrate as dissolved Fe (dFe) and soluble Fe (sFe), respectively. The difference between dFe and sFe will be assumed to correspond to the colloidal Fe concentration.

2.9. Interpolation, used parameters, analysis and inference limitation.

2.9.1. Interpolation-extrapolation of initial values.

The initial condition for the four incubated groups (G1 to G4) of three treatments (control, +Fe and + Fe + Si) were interpolated/ extrapolated assigning station 25 as t = 0 of G1, the average value of Sts. 25–26 and Sts. 26–27 as t = 0 for G2 and G3, respectively, and assigning station 27 values as t = 0 for G4, the merits of this method of "running interpolation" can be seen in the agreement between dashed lines and black filled circles in Figs. 4, 6-8, 10 and 12.

2.9.2. Parameters and data reduction rationality

We signal the difference of response variables nitrate, phosphate, DSi, pH subtracting the respective initial values (t = 0 days) from corresponding end values (t = 3 days) of each experimental bottle, shown as Δ. e.g. $\Delta\ NO_3^- = [NO_{3(t=3)}^- - NO_{3(t=0)}^-]$.

Response was expected to be dependent on initial conditions, which in turn may vary between experimental groups. We therefore define the accumulation parameter (Σ) as the coefficient between the variation rate of the response variable (Δ response variable / 3 days) and the response variable at the corresponding t = 0. e.g. Σ Chla = (ΔChla/3 days)/ $Chla_{(t=0)}$, with units (day^{-1}).

In the specific case of dFe (which was measured only at t = 3) we utilize a unitless parameter (Σ_c) to show the magnitude dFe variation (between iron enriched treatment and control) relative to dFe at the control, E.g.. $\Sigma_c\ dFe = [dFe_{(t=3;\ +Fe)} - dFe_{(t=3,\ control)}]/\ dFe_{(t=3,\ control)}$.

2.9.3. Experimental design: assumption/limitations and interpretation of results.

In order to prevent metal contamination from the vesseĺs hull, the collection of seawater for experimentation was done while steaming using a single clean sampling device (see Section 2.2). Although surface

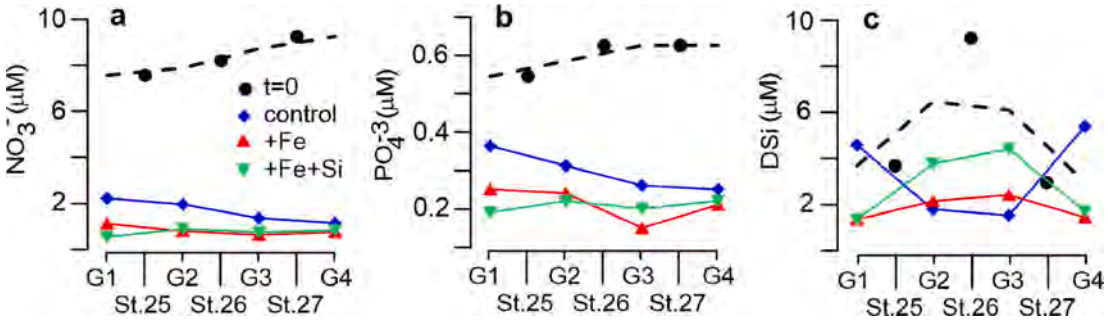

Fig. 4. Surface water nitrate, phosphate and DSi at the start (t = 0) and after three days of "on-deck" incubation (t = 3). Dots depict the surface water concentration of macronutrients and DSi within the East-West transect where experimental carboys (G1-G4) were filled. Coloured symbols depict the concentration of macronutrients and DSi (in controls and in Fe and Fe + Si treatments) after 3 days of "on-deck" incubation. Dashed line corresponds to the interpolated t = 0 values that were used for the calculation of macronutrients drawdown for each group of carboys (G1-G4), see Fig. 4.

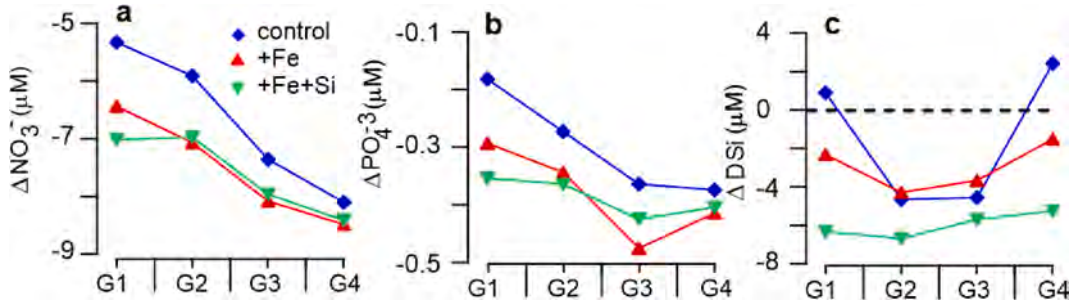

Fig. 5. Nitrate, phosphate, and DSi drawdown during the incubation period (3 days). Negative values indicate drawdown and positive values indicate gain.

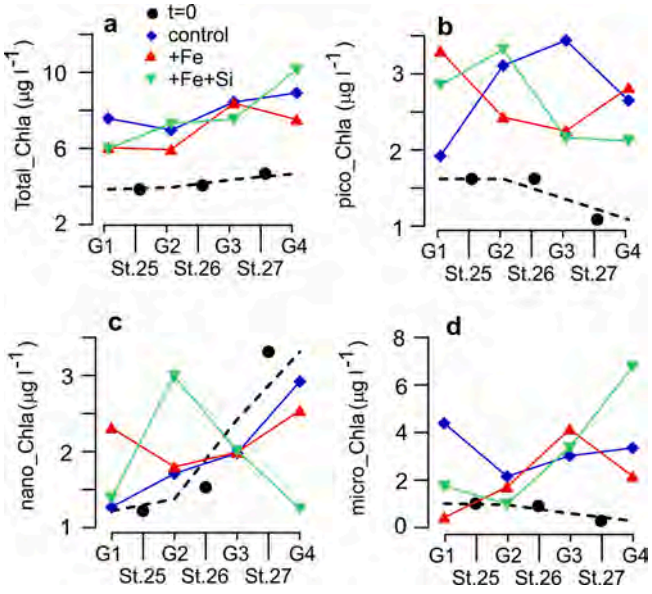

Fig. 6. Surface water total chlorophyll *a* in three size ranges (pico, nano, and micro) at t = 0 and after three days of "on-deck" incubation. Dots depict the chl a within the East-West transect stations (Sts. 25–27) where experimental carboys (G1-G4) were filled. Colored symbols depict the concentration of chl a (in controls and in dFe and dFe + DSi treatments) after 3 days of "on-deck" incubation. The dashed line corresponds to the interpolated t = 0 values that were used for the calculation of the chl a accumulation for each group of carboys (G1-G4).

seawater sampling within each experimental group was virtually simultaneous, changes in the characteristics of surface water across Concepcion Channel (CC), discussed in Section 4.2, preclude considering experimental groups (G1-G4) as replicates.

The accumulative effect (3-day experiment) of the spatial variability of seawater properties across CC has the potential to lead to large differences in standing stock response by means of top-down (e.g. grazing variability between experimental groups) and bottom-up processes (e.g. nutrient variability between experimental groups). The data analysis is therefore be based on the differences between treatments and corresponding controls between treatment and controls (i.e. when all four experimental groups, G1 to G4, show the same pattern) as an increment (+Δ) or a reduction (-Δ) of a response variable. Inconsistent differences between treatment and controls between experimental groups are also analyzed and discussed, searching for potential relationships between the differences between control and treatments of a given response variable with the chemical- biological peculiarities across the CC environmental gradient where surface water was collected (i.e. t = 0 spatial gradients). This last analysis is based upon the statistical significance of the correlation between the experimental response variables and environmental gradient descriptors.

3 Results

3.1. Spatial variability of biogeochemical parameters in the southern portion of the PAIS (53.5°S-50.5°S) during austral spring 2017

Surface waters along the transect exhibited low salinity values (salinity 25–30, Fig. 2a) compared to fully oceanic SAASW off Patagonia during austral spring (salinity 33–34, (Palma & Silva, 2004)). The percentage of fresh water in surface water (FW) along the transect ranged between 9% and 24%, assuming a two-points dilution curve of terrestrial and marine waters with salinities of 0 and 33.5, respectively. Specific runoff during August and September 2017 near sampling stations (see Sup. Mat A methodology and Figs. 1 and 2a) was negatively correlated to salinity (R = -0.4; p = 0.03) and nitrate (R = -0.4; p = 0.02) and positively correlated to SST (R=+0.6; p < 0.01) and the percentage of chl a allocated in micro-size range (R=+0.5; p = 0.04).

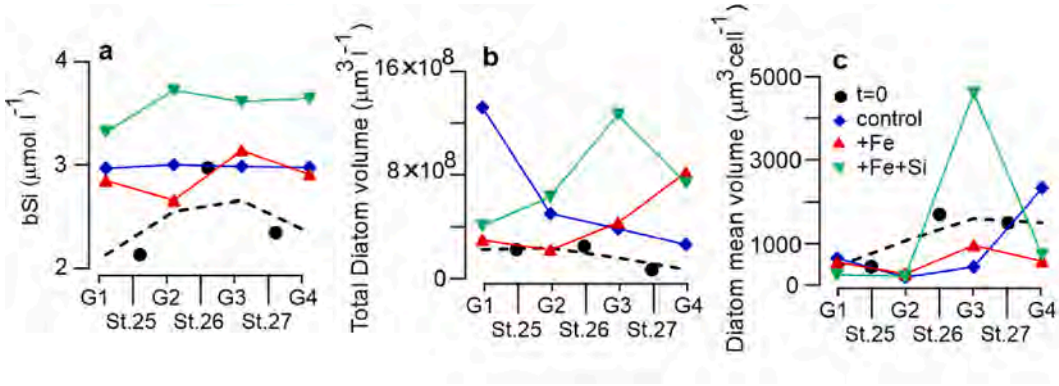

Fig. 7. Surface water bSi, total diatom volume, and diatom mean volume at t = 0 and after three days of "on-deck" incubation. Dots depict the last variables within the East-West transect stations (Sts. 25–27) where experimental carboys (G1-G4) were filled. Colored symbols depict the variable levels (in controls and in Fe and Fe + Si treatments) at t = 3 of "on-deck" incubation. The dashed line corresponds to the interpolated t = 0 values that were used for the calculation of the accumulation parameter for those variables.

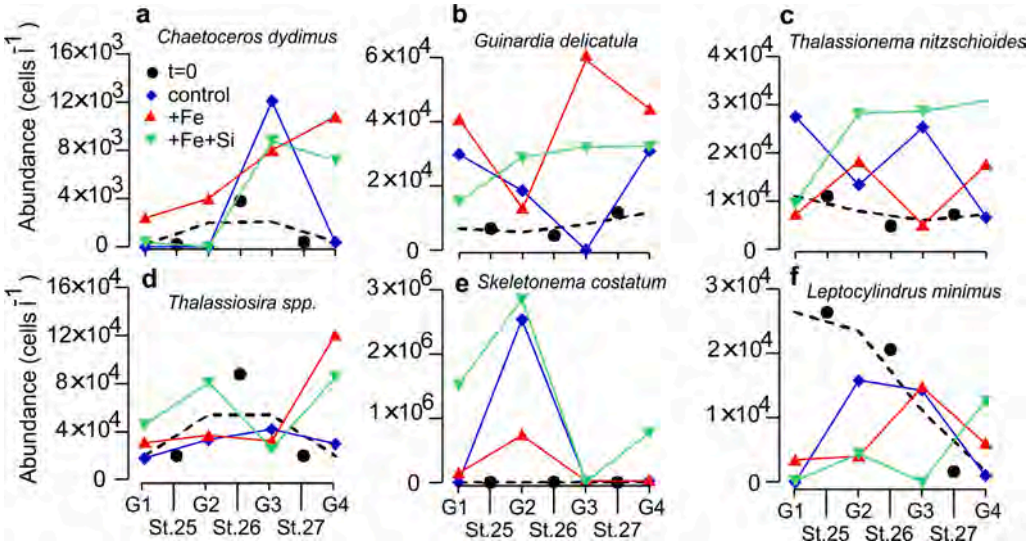

Fig. 8. Selected diatom taxas from surface water at t = 0 and after three days of "on-deck" incubation. Dots depict the abundance of selected taxas within the East-West transect stations (Sts. 25–27) where experimental carboys (G1-G4) were filled. Colored symbols depict the taxońs abundance (in controls and in Fe and Fe + Si treatments) after 3 days of "on-deck" incubation. The dashed line corresponds to the interpolated abundance of the shown diatom taxa at t = 0.

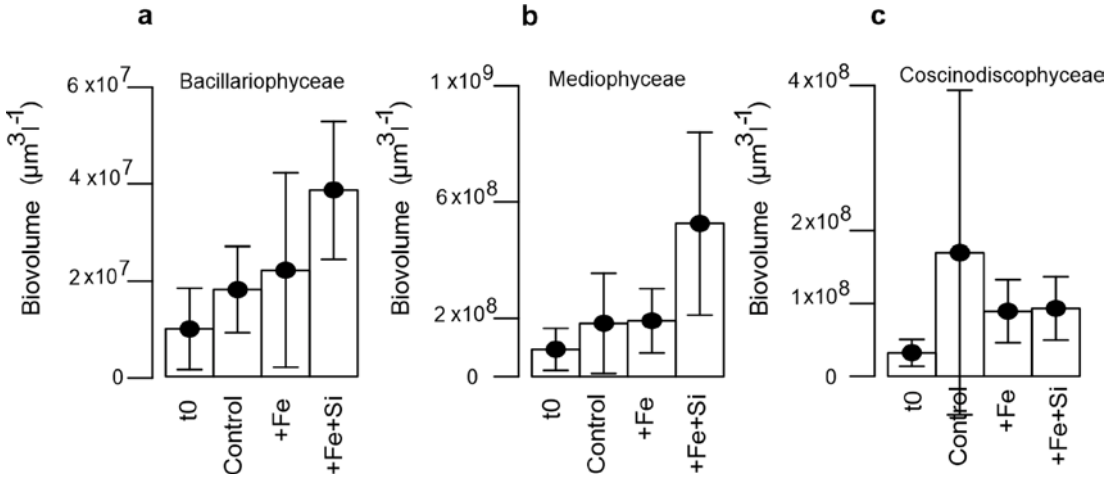

Fig. 9. Total diatom volume (biovolume) at t = 0 and after three days (control, +Fe and + Fe + Si) of "on-deck" incubation. Bars indicate standard deviation.

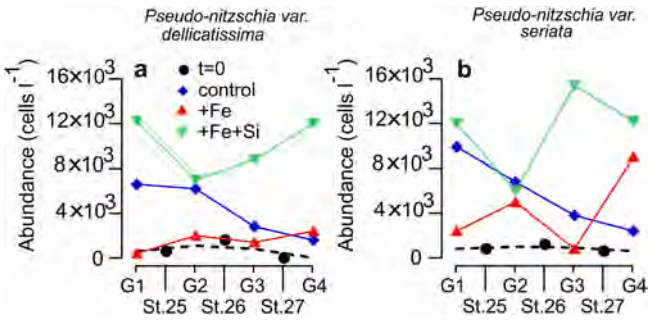

Fig. 10. Pseudo-nitzschia spp. at t = 0 and after three days of "on-deck" incubation. Dots depict the abundance of Pseudo-nitzschia spp. within the CC East-West transect where experimental carboys (G1-G4) were filled. Colored symbols depict the abundance of Pseudo-nitzschia spp (in controls and in + Fe and + Fe + Si treatments) after 3 days of "on-deck" incubation. The dashed line corresponds to the interpolated abundance of the shown diatom taxa at t = 0.

The surface water with the lowest proportion of FW (i.e. Sts. 1, 28 and 29; salinity ca. 30, Fig. 2a) have the highest levels of nitrate and phosphate (12 ± 0.7 μM and 1.0 ± 0.0 μM respectively; Fig. 2b), and low to moderate levels of DSi (4.9 ± 0.4 μM; Fig. 2c) and biogenic silica (1.4 ± 0.4 μM; Fig. 2c) with particularly low (negative) Si* values (Fig. 2f) even when dissolved and biogenic silica were summated to estimate a proxy of the potential Si* (i.e. [DSi + bSi] $-NO_3^-$). Total-chl a concentration in high salinity surface waters (ca. 30) was 1.1 ± 0.3 μg l^{-1} (Fig. 2d), mostly contained in the pico and nano size fractions (Fig. 2d, also see Fig. 2i). pCO_2 of these high salinity water was slightly undersaturated (387 ± 8 μatm; Fig. 2e) relative to atmospheric levels (likely near 403 ppm, see https://www.esrl.noaa.gov/gmd/ccgg/trends/) and saturated with respect calcium carbonate in the form of aragonite (Omega aragonite ranging from 1.4 to 1.5 approximately, Fig. 2e). Samples for dFe and dMn were not collected in waters with salinities>28, however dFe and dMn were measured in surface waters of salinity 29.3 collected for the incubation experimentation blank in St.27 and were 6 nM dFe and 5 nM dMn (after 3 days of incubation). In stations 11 (salinity 26) and 15 (salinity 27) we analyzed dFe (12 and 17 nM, respectively) and sFe (5 and 3 nM, respectively), suggesting that most the dFe (59 and 79%, respectively) was in the colloidal size fraction

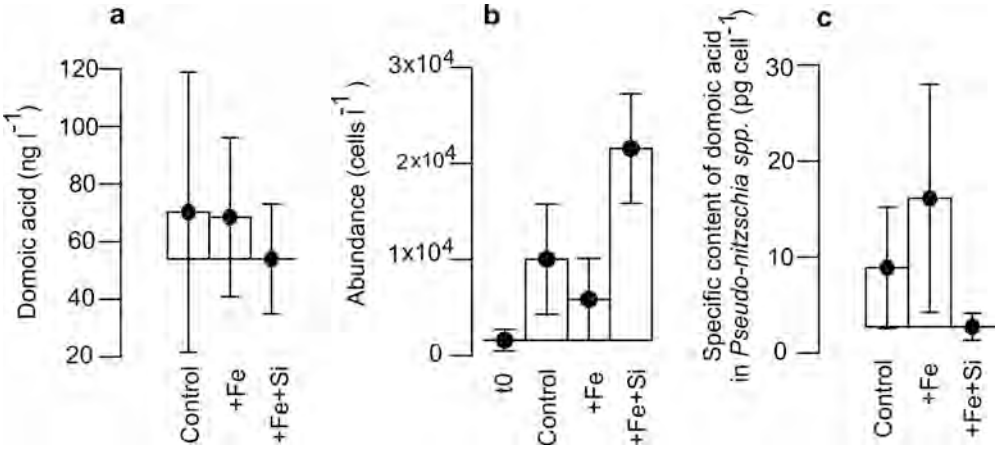

Fig. 11. Average values of cellular Domoic acid, Pseudo-nitzschia abundance and DA normalized by Pseudo-nitzschia abundance at t = 0 and after three days (control, +Fe and + Fe + Si). Bars indicate standard deviation.

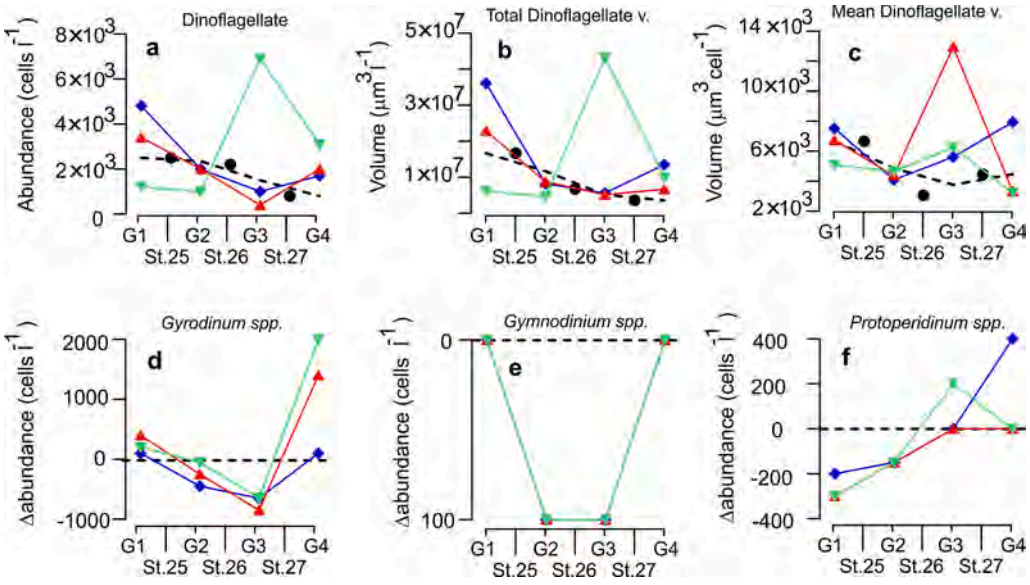

Fig. 12. Surface water dinoflagellate abundance (a), Total volume of dinoflagellates (b), Mean dinoflagellate volume (c) at t = 0 and after three days of "on-deck" incubation. Variation (Δ = t3-t0) in the abundance of selected dinoflagellate taxon's (d-f).

(i.e. between 0.45 μm and 0.02 μm in size).

The pH (at temperature in situ) and SST of higher salinity surface water values (corresponding to station 1, 28 and 29) ranged from 8.01 to 8.03 pH units and from 7.1 to 8.0 °C, respectively (Fig. 2h). These stations were also characterized by very low levels of micro-chl a (<0.4 μg l^{-1}, Fig. 2i) and micro-phytoplankton abundance (<4 × 10^{-3} cell l^{-1}, 2j).

The maximum contribution of FW (~22%) was observed ca. 52.0°S (see St.12–13, Fig. 1; Salinity < 26, Fig. 2a) corresponding to the influence of Southern Patagonia Ice Field and the Rio Serrano the only major hydrographic basin that connect to the study area through Montt Gulf and Kirke channel (see Fig. 1). These brackish waters were also high in nitrate and phosphate (~10 μM nitrate, ~0.8 μM phosphate; Fig. 2b), with moderate levels of DSi (~6 μM; Fig. 2c), biogenic silicate of ~ 1.3 μM (Fig. 2c) and relatively low total-chl a levels (~1.3 μg l^{-1}; Fig. 2d) corresponding mainly to the nano size fractions (~0.9 μg l^{-1}; Fig. 2d). pCO_2 levels of this low salinity water were virtually in equilibrium with the atmosphere (405-409μatm; Fig. 2e) and characterized by the undersaturation of surface water with respect calcium carbonate in the form of Aragonite (Omega aragonite < 0.93; Fig. 2e) and by the highest Si* values (Si*~0 μM, Fig. 2e). This low salinity water (St.11) has dFe and dMn concentrations of 21 nM and 12 nM respectively (Fig. 2g). SST, pH at in situ SST and micro-chl a were relatively low (6.5 °C, 7.96 pH units, ~0.4 μg l^{-1}, respectively. See Fig. 2h and 2i).

The largest concentrations of biogenic silicate (2.5 ± 0.4 μM; Fig. 2e) and total-chl a (3.5 ± 0.4 μg l^{-1}; Fig. 2f) were found at intermediate salinities (approximately between 27 and 29) adjacent to relatively salty water (>29). These large stock maximums coincided with lower concentrations of nitrate, phosphate, DSi, and pCO_2 (9 ± 2 μM nitrate, 0.7 ± 0.2 μM phosphate, 2.9 ± 1.1 μM dissolved silicate and 350 ± 24 μatm, respectively; Fig. 2b-c and 2e).

In general, nitrate, phosphate and pCO_2 were negatively correlated to chl a in the micro size range (Table 1). Macronutrients and the amount of chl a in pico and nano size range were not correlated (Table 1) although the mean concentration of both pico-chl a (1.1 ± 0.5 μgl^{-1}) and nano-chl a (1.0 ± 0.5 μgl^{-1}) were ~ 2 fold larger than micro-chl a (0.5 ± 0.6 μgl^{-1}). Total-chl a was better correlated with DSi (negatively) and bSi (positively) than any particular size fraction of chl a.

Micro phytoplankton composition analyzed in stations 1, 6, 16, 17, 25–29 were largely dominated by diatoms, but with a large variability along the transect. Minimum abundances were found at St.1 (ca. 1x10^3 cell l^{-1}) and maximum at St. 27 (ca. 5 x10^5 cell l^{-1}), mostly corresponding to the class Mediophyceae (e.g. *Thalassiosira*, *Chaetoceros*, *Leptocylindrus,* and *Skeletonema* genus; data not shown). Dinoflagellates represented between 0.5 and 8 % of micro-phytoplankton abundance, with densities that did not exceed 4x10^3 cell l^{-1} (data not shown). Scanning Electron Microscopy (SEM) imagery for stations 1, 4, 7, 8, 12, 15, 17, and 23 showed the presence of very small free centric diatoms of a mean diameter of 2–3.5 μm (*Minidiscus spp*., see Supplementary material B) co-occurring with the coccolithophore *Emiliania huxleyi* with abundances ranging between 1.3 ×10^5-1.4 ×10^6 and 1.7 ×10^4- 9.1 ×10^5 cell l^{-1}, respectively (Fig. 2k; $n = 11$ stations). The micro-phytoplankton were dominated by diatoms, however the biogenic silicate in particles > 2 μm were not correlated to the content of micro-chl a but correlated with total-chl a, pico-chl a and nano-chl a (Table 1).

The pCO_2 along the transect was positively correlated to nitrate, phosphate and dissolved silicate (R^2: 0.7, 0.6 and 0.7 respectively; p-value < 0.005) and negatively correlated with micro-chl a and total-chl a (Table 1). pH and A_T in surface waters ranged from 7.95 to 8.11 pH units and from 1742 to 2068 μmol Kg^{-1} respectively (data not shown). A_T was strongly correlated to salinity ($R^2 = 0.96$). Surface waters with salinity lower than 26.5 were virtually in equilibrium with the atmosphere ($pCO_2 = 409 \pm 4$uatm, Fig. 2j) but undersaturated with respect to calcium carbonate in the form of Aragonite (Fig. 2l).

3.2. dFe and dFe + DSi enrichment incubations

3.2.1. Initial conditions

Sea surface water used in the iron enrichment experiment was collected over salinities from 28 to 29, characterized by high levels of total-chl a (3.9–4.7 μg chl a l^{-1}) and low chl a percentage (6%-26%) in the micro size-range. The diatom abundance ranged between 4x10^4 and 5x10^5 cell l^{-1}. Diatom mean volume, bSi, and DSi ranged from 400 −1600 μm^3 $cell^{-1}$, 2–3 μmol Si l^{-1} and 3–9 μM, respectively. The concentration of nitrate and phosphate ranged from 7.6 − 9.2 μM and 0.5–0.6 μM respectively. The pCO_2 calculated from pH-A_T pairs suggests that this water was undersaturated relative to the atmosphere (Fig. 13), ranging between 324 μatm and 354 μatm. Salinity, total -chl a, nitrate, phosphate, and pCO_2 tended to increase westward from St.25 to St.27, but micro-chl a and diatom abundance tended to decrease (see dashed line in Fig. 6). Diatom mean volume, bSi and DSi reached a relative maximum at the middle station (i.e. St.26). Dissolved iron was only measured at the end of the experiment (t = 3; Fig. 3). The final mean increments of total dissolved iron (dFe) in + Fe enriched treatments relative controls was ca. 1 nM but highly variable between bottles, representing a moderate increment from the control levels (20–25 %) and only the 20 % of the intended Fe enrichment (i.e. 1 of 5 nM).

Table 1
Pearson correlation coefficient between standing stock of chl a and environmental variables for the transect shown in Fig. 1. N = 17. Marked correlations are significant at p < 0.050.

	T_Chla	Pico	Nano	Micro	%pico	%nano	%micro
Sal	0,0317	0,3372	0,164	−0,3895	0,5257	0,0222	−0,6337
	p=,904	p=,186	p=,529	p=,122	p=,030	p=,932	p=,006
Specific	−0,2806	−0,2923	−0,4638	0,2241	−0,0895	−0,3547	0,5039
runoff	p=,275	p=,255	p=,061	p=,387	p=,733	p=,162	p=,039
pH	0,5471	0,4096	0,2456	0,6937	0,0198	−0,3246	0,3433
at 25 °C	p=,023	p=,103	p=,342	p=,002	p=,940	p=,204	p=,177
A_T	−0,0172	0,2341	0,1919	−0,4441	0,4425	0,1257	−0,6541
	p=,948	p=,366	p=,461	p=,074	p=,075	p=,631	p=,004
NO_3^-	−0,3796	−0,0636	0,0292	−0,8472	0,3211	0,4131	−0,8379
	p=,133	p=,808	p=,911	p=,000	p=,209	p=,099	p=,000
PO_4^{3}	−0,4808	−0,0771	−0,1506	−0,8572	0,3765	0,2916	−0,7649
	p=,051	p=,769	p=,564	p=,000	p=,136	p=,256	p=,000
DSi	−0,7947	−0,6728	−0,3838	−0,6872	−0,0989	0,3735	−0,3069
	p=,000	p=,003	p=,128	p=,002	p=,706	p=,140	p=,231
bSi	0,7548	0,7195	0,5770	0,1964	0,0646	0,0918	−0,1783
	p=,000	p=,001	p=,015	p=,450	p=,806	p=,726	p=,493
pCO_2	−0,5937	−0,4211	−0,1571	−0,8292	0,0666	0,4287	−0,5609
	p=,012	p=,092	p=,547	p=,000	p=,799	p=,086	p=,019
Si*	−0,1383	−0,4226	−0,3187	0,4954	−0,4538	−0,2132	0,7659
	p=,596	p=,091	p=,212	p=,043	p=,067	p=,411	p=,000

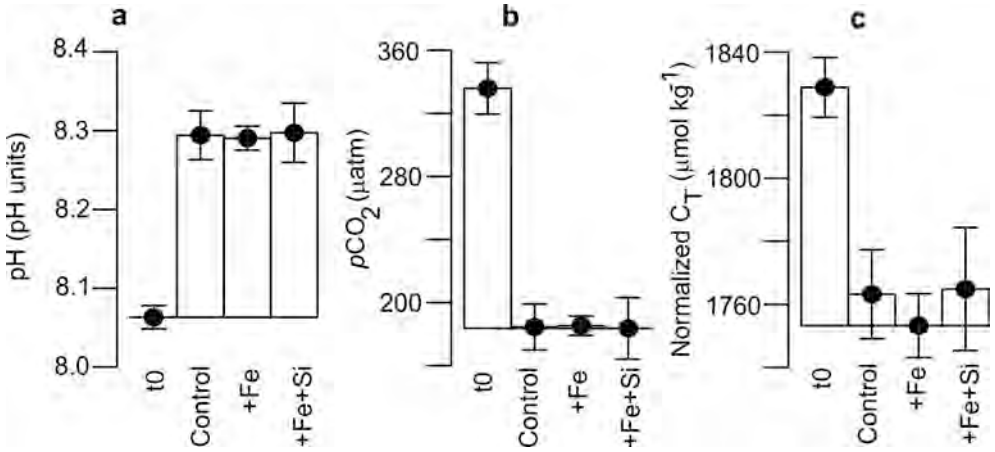

Fig. 13. Ph at a temperature in situ, pco_2 and dissolved inorganic carbon standardized to salinity 28.8 at t = 0 and after three days (control, +Fe and + Fe + Si) of "on-deck" incubation. Bars indicate standard deviation.

3.2.2. Macronutrients and DSi drawdown

The concentrations of nitrate and phosphate at the end of the incubation period (t = 3) were low relative to t = 0, reaching minimum levels in the iron enriched treatments (+Fe and + Fe + Si treatments) compared to controls. DSi concentrations in t = 0 and t = 3 were highly variable, with the exception of + Fe treatment at t = 3 where DSi levels were consistently close to 2 µM.

Nitrate drawdown (ΔNO_3^-) at + Fe and + Fe + Si treatments was enhanced by 13% and 14% respectively relative to the control (Fig. 4a). Maximum ΔNO_3^- occurred at G4 (western side of CC transect), however, the maximum difference in ΔNO_3^- between controls and + Fe treatments seems to occur in G1-G2 (eastern side of the CC transect, Fig. 4a). A similar pattern followed phosphate drawdown in + Fe and + Fe + Si treatments, with drawdown enhanced by 28% and 30% respectively relative to the control (Fig. 4b).

In general, the nitrate drawdown and phosphate drawdown relationship was linear and positive ($\Delta NO_3^- = 11.9 \times \Delta PO_4^{3-} - 3$, $R^2 = 0.8$, n = 12, $p < 0.005$); the calculated slope (i.e. 11.9) was fully consistent with mean drawdown ratio reported for diatom-dominated Antarctic waters (Arrigo, Dunbar, Lizotte & Robinson, 2002). Total inorganic carbon drawdown and phosphate drawdown were not correlated ($\Delta C_T = 99.2 \times \Delta PO_4^{3-} + 28$, $R^2 = 0.2$, n = 12, p = 0.17). Similarly, the nitrate drawdown and DSi drawdown were not correlated ($R^2 = 0.01$). The nitrate/ DSi drawdown ratio was 1.3 ± 0.3 (n = 4) at + Fe + Si treatments and 3 fold larger in + Fe treatments (3.0 ± 1.7, n = 4). Indeed, the ΔDSi drawdown reached a maximum in the + Fe + Si treatment (ca. 6 µM, assuming that the added DSi was not polymerized). DSi drawdown was similar in the + Fe and control incubations at G2 and G3, but significantly different at G1 and G4, where a small DSi increase in controls occurred relative t = 0 levels (ΔDSi ca. + 2 µM; Fig. 4c).

3.2.3. Chlorophyll a

The mean concentrations of total chl a doubled after 3 days incubation, associated mainly with phytoplankton growth in the pico and micro size fractions. No consistent differences between treatment and control were observed, with the exception of relatively low total chl a levels in + Fe treatments relative to controls (Fig. 6a). Spatial patterns were evident for total chl a, e.g. it was relatively low in G1 and G2 compared to G3 and G4 at both t = 0 and t = 3 (Fig. 6a). Additionally, in t = 0 and controls (no nutrient enrichment), nano-chl a increased from G1 to G4 (Fig. 6c). Micro-chl a in Fe-enriched treatments was higher in G3 and G4 relative to G1 and G2, with the exception of the G1 control (Fig. 6d).

3.2.4. Biogenic silicate, diatom total volume

The bSi was higher in + Fe + Si than in + Fe and the control (Fig. 7a). The total diatom volume was variable but higher in the control and + Fe + Si treatments at t = 3 compared to t = 0, (Fig. 7b). The diatom mean volume was variable but tended to be small and less variable in G1 and G2 compared to G3 and G4 (Fig. 7c), note that diatom mean volume tend to be smaller at t = 3 compared to t = 0, with the exception of + Fe + Si G3 and control G4 (Fig. 7c).

Diatom abundance was highly variable and different between taxa (Fig. 8). No consistent differences were detected with the notable exception of *Pseudo-nitzschia,* as described in the Section 3.2.5.

In general, the mean relative contribution of diatom classes to the total biovolume shown little variability, with the exception of + Si + Fe treatment, which seems to suggest increased contribution of Mediophyceae and reduced the influence of Coscinodiscophyceae (Table 2). Bacillariophyceae contribution to diatom biovolume was low (ranging between 3% and 6%), but twice as large in + Fe + Si relative to control. The total diatom biovolume was variable, but for Mediophyceae and Bacillariophyceae was larger in + Fe + Si treatment compared to t = 0 (Fig. 9).

3.2.5. Pseudo-nitzschia and cellular domoic acid

Bacillariophyceae abundance was dominated by relatively small *Pseudo-nitzschia* var *seriata* and *delicatissima*, which show a sharp increase from t = 0 to t = 3 in control and + Fe + Si treatment but not + Fe treatment (Fig. 10). From all 22 diatom taxa identified, only *Pseudo-nitzschia* var. *dellicatissima* (Hasle et al., 1996) was consistently higher in + Fe + Si treatment relative to controls. *Pseudo-nitzschia* var. *dellicatissima* abundance at + Fe treatment was close to t = 0 abundances.

Domoic acid (DA), a neurotoxin attributed to the diatom genus *Pseudo-nitzschia*, was highly variable and not correlated with *Pseudo-nitzschia* abundance. However, the DA per *Pseudo-nitzschia* cell was very low and constant in the + Fe + DSi treatment relative to both the control and + Fe treatment (Fig. 11).

3.2.6. Dinoflagellates

The abundance of dinoflagellates, their total volume and mean

Table 2
Relative contribution of diatom classes (Bacillariophyceae, Mediophyceae and Coscinodiscophyceae) to total diatom biovolume at t = 0 and t = 3 (control, +Fe and + Fe + Si).

	% Bacilliophyceae	% Mediophyceae	% Coscinodiscophyceae
t0	5.2 ± 2.3 (n = 3)	75 ± 12 (n = 3)	19 ± 13 (n = 3)
Control	3.3 ± 0.9 (n = 4)	75 ± 11 (n = 4)	22 ± 12 (n = 4)
+Fe	4.7 ± 4.7 (n = 4)	76 ± 7 (n = 4)	20 ± 20 (n = 4)
+Fe + Si	6.2 ± 4.8 (n = 4)	88 ± 8 (n = 4)	11 ± 7 (n = 4)

volume were variable, with positive and negative net changes with respect to t = 0 (Fig. 12a-c). Naked dinoflagellates, (*Gyrodinium* spp., *Gymnodinium* spp.; Fig. 12d-e) reduce their abundance in G2 and G3 relative t = 0. The abundance of *Gyrodinium spp*. in Fe enriched treatments increased at G1 and G4 (Fig. 12d). The abundance of *Gyrodinum spp*. was consistently larger at + Fe + Si treatment relative to controls (Fig. 12d). The thecate dinoflagellate *Protoperidinum* only showed an increase in its abundance at G3 (+Fe + Si treatment) and at G4 (control) (Fig. 12f).

3.2.7. Carbonate system parameters

pH measured at 25.0 °C increased by ca. 0.22 pH units in both Fe enriched treatments and controls (Fig. 13). The range of measured pH in control, +Fe and + Fe + Si bottles at t = 3 were small (0.09, 0.05 and 0.07 pH units, respectively).

The A_T normalized by salinity was higher in t_3 compared to t_0 (ΔA_T = 27, 14 and 16 μmol kg^{-1} in control, + Fe and + Fe + Si treatment, respectively). The ΔA_T corrected for nitrate consumption (i.e. ΔA_T + ΔNO_3) was 20, 6 and 9 μmol kg^{-1} in control, + Fe and + Fe + Si treatments, respectively.

3.2.8. Relationship between response variables

Nitrate drawdown was negatively correlated to nitrate concentration at t = 0 in treatments and controls. Superimposed on this last general trend, the maximum nitrate drawdown levels take place in + Fe and + Fe + Si treatments (Fig. 14a). No correlation was found between the increase dFe and nitrate decline relative corresponding controls (Fig. 14b), however maximum dFe increase and a large reduction of nitrate relative to controls occurred at G4 + Fe + Si treatment (Fig. 14b-c). The increase in micro-chla and dFe in iron enriched treatments relative to corresponding controls (see method section 2.8.2) were positively correlated (R^2 = 0.73, p = 0.006, n = 8; Fig. 14c). In general, nitrate drawdown was negatively correlated with micro-chl a accumulation (Fig. 14d), the accumulation of micro-chl a per mol of nitrate was particularly high in controls (Fig. 14d). The accumulation of nano-chl a only occurred when the accumulation of micro-chl a was low or null (Fig. 14e). Biogenic silica accumulation (in particles > 2 μm) was positively correlated with diatom biovolume accumulation only in controls (Fig. 14f). In the + Fe and + Fe + Si treatments, the accumulation of biogenic silica was not associated with the accumulation of diatom biovolume (Fig. 14f). The accumulation of bSi tended to be

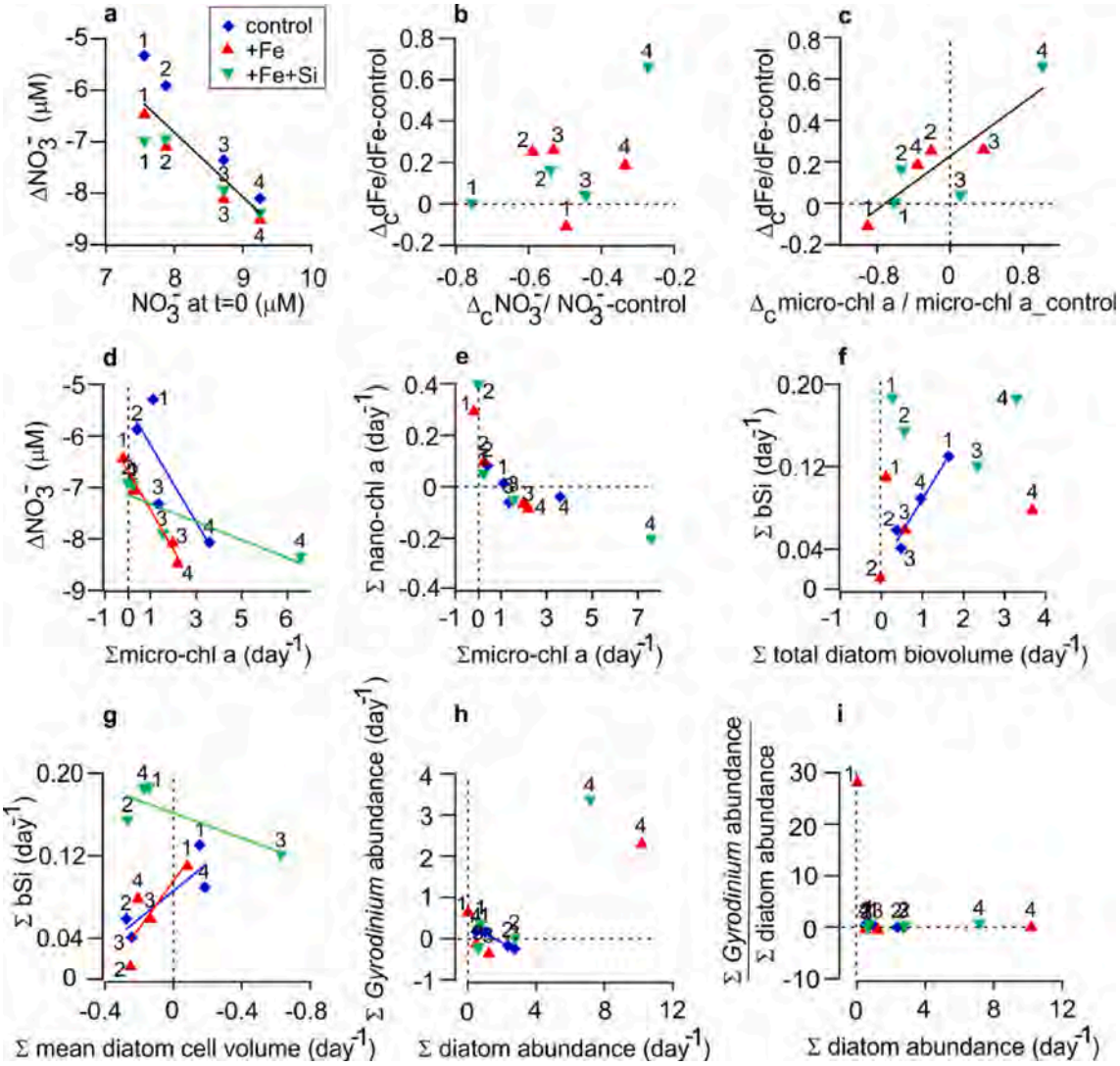

Fig. 14. Relationship between response variables, numbers indicate the experimental group. (a) Nitrate drawdown vs. nitrate concentration at the beginning of the experiment. (b) dFe Σ_C vs. Nitrate Σ_C (c) dFe Σ_C vs. micro-chl a Σ_C, solid line depict a regression, (d) Nitrate drawdown vs. micro-chl a accumulation. (e) Nano-chl a accumulation vs. micro-chl a accumulation. (f) biogenic silica accumulation vs. diatom abundance accumulation. (g) biogenic silica accumulation vs. mean diatom cell volume accumulation. (h) Gyrodinium spp abundance accumulation vs. diatom abundance accumulation. (i) ratio between Gyrodinium spp abundance accumulation and diatom abundance accumulation vs. diatom abundance accumulation.

higher when the mean volume of the diatoms increased in + Fe and controls (Fig. 14g). However, in + Fe + Si treatment, the accumulation of bSi was high even when the mean volume of the diatoms decreased (Fig. 14g). The accumulation of *Gyrodinium* spp. cells and the accumulation of diatoms were highest in G4 in + Fe and + Fe + Si treatments. The accumulation of *Gyrodinium spp* was inversely correlated with the total accumulation of diatoms in controls (Fig. 14h). The ratio of accumulation between *Gyrodinium spp* and diatoms was maximum at + Fe G1 (Fig. 14i). This carboy (+Fe G1) was also characterized by loss of micro-chl a (Fig. 14d) and accumulation of nano-chl a (Fig. 14e).

4. Discussion

4.1. Iron-enhanced new productivity in estuarine waters of southern Patagonia

The general rapid drop in macronutrient (nitrate, phosphate, and C_T) concentrations in both control and Fe-enriched treatments relative to initial conditions suggest that very high levels of new productivity were most likely associated with alleviation of any light limitation due the on-deck incubation that emulates an extreme stratification condition (see Fig. 1 in de Baar et al. (2005)), together with already high initial levels of chlorophyll of the surface water used for the experiment (total-chl a ~ 4 μg l^{-1}). The initial experimental conditions (undersaturated levels of CO_2, moderate levels of macronutrients) suggest a micro-phytoplankton bloom was in its developing phase at the sampling time, particularly near station 25, where relatively low salinity and macronutrients levels (Fig. 4a-b) and high micro-chl a levels (Fig. 6d) were recorded; The higher nitrate (and phosphate) drawdown in all Fe-enriched carboys relative to controls (Fig. 5a-b), suggest that the addition of unchelated Fe was the factor inducing higher macronutrients drawdown levels. Since nitrate: phosphate drawdown ratio (see section 3.2.2.) was consistent with what has been reported for high latitude diatom-dominated waters (Arrigo et al., 2002), we suggest that macronutrients drawdown reported here was mainly due to diatom new production. However, the dFe:nitrate ratio (mmol mol^{-1}) in estuarine surface waters varied between 0.4 and 4, several orders of magnitude higher than the expected phytoplankton cellular Fe:nitrate ratio for fjord waters (Kanna et al., 2020) suggesting no iron limitation. Therefore, we conclude that only a fraction of the ambient dFe is bioavailable or readily bioavailable for phytoplankton. i.e. the amount of bioavailable Fe was higher in those treatments enriched with unchelated iron, enhancing new productivity and therefore causing a significative acceleration in the nitrate and phosphate drawdown.

The enhanced productivity in Patagonian estuarine waters after a 5 nM Fe enrichment was small compared to previous experiments carried out in HNLC coastal upwelling areas off central Chile during austral spring (Torres and Ampuero, 2009; Ampuero, 2007). This difference was likely a result of chla-rich waters in our study (although most of it was allocated in the pico and nano size fraction) and not with HNLC coastal waters as determined in Torres and Ampuero (2009). We hypothesize that events of iron stress in coastal water are potentially more severe in recently upwelling waters of central Chile, which are typically low in chl a (<1 μg l^{-1}), high in nitrate and silicate, and low in dFe (ca. 1.4 nM), compared to PAIS surface waters. We note that dFe concentration of PAIS surface waters were high (particularly at salinity < 29) but likely not readily available to fully meet potential maximum rates of macronutrient uptake / new productivity under blooming conditions.

4.2. The role of initial conditions and grazing pressure on Fe enrichment experiments

The experimental groups (G1-G4) were collected over a salinity, macro-nutrient, micro-chl a, and dFe gradient that may represent a changing "age" or "maturity" of the diatom community along the CC E-W transect. While the early stage of the diatom bloom appears located in the salty water of the western CC portion (e.g. relative high nitrate, low micro-chl a and low dFe in G4), a more mature diatom community was observed at the CC east stations (e.g. relative low nitrate, high micro-chl a and high dFe in G1). Since an Fe pulse has the potential to increase the maximum potential uptake rate (V-max) of both DSi and nitrate (Franck et al., 2003) we expected that the sudden relief of Fe stress in an already large "mature" diatom community (e.g. G1 at t = 0) resulted in early resource limitation relative to controls, which could explain the occurrence of low diatom stock in + Fe relative controls at eastern portion of the transect (i.e. G1 and G2). On other hand, the gain (positive accumulation) of micro-chl a and total diatom volume after an iron pulse at western portion of the CC transect (e.g. G4 + Fe) suggest a diatom standing stock builtup (i.e. increase diatom production/diatom mortality ratios).

In general, we suggest that the impact of iron pulses on diatom stock in a given period of time could be dependent on the developing stage of the diatom bloom, this last dependency can explain the contrasting effect of iron addition on micro-chl a accumulation and total diatom volume at the two extremes of the transect (i.e. G1 vs. G4). Complementary, no differences between bSi accumulation in controls and + Fe treatment, suggest that new productivity enhanced by Fe addition was independent to diatom bSi accumulation. If new production was mostly driven by diatoms, the rise in diatom standing stock (e.g. G4) should correspond to small or thin diatom in + Fe relative controls. Indeed, blooming diatoms were typically small of the class Mediophyceae. Blooming of small/thin diatoms could be particularly vulnerable to protozoan grazers that select for diatoms with thin frustules (Zhang et al., 2017). Accumulation of micrograzers in G1 and G4 suggest that micrograzing pressure was intense in those experimental groups. Micrograzer pressure could be particularly intense in G1 where accumulation of *Gyrodinum* spp. (the dominant naked dinoflagellate group) was substantially larger compared to the accumulation of diatom biovolume (which indeed was null or negative in G1, see Fig. 7b). The accumulation of *Gyrodinum spp* in G1-control and G4-control coincide with a small increase in DSi (relative t = 0; Fig. 5c).

4.3. + Fe + Si enrichment experiment outputs: bSi, Pseudo-nitzchia and domoic acid

Silicic acid uptake by diatoms likely explains the rapid DSi shortage even in + Fe + Si treatments. bSi accumulation and *Pseudo-nitzschia var dellicatissima* abundance were consistently greater in + Fe + Si incubations relative to + Fe and controls. Since the "poorly silicified" *Pseudo-nitzchia* sp. *cf. dellicatissima.* represent<1% of the total diatom abundance and<0.2% of the total diatom biovolume, the increase in bSi was likely associated with the frustules of the Mediophyceae and Bacilliophycea rather than a small increase in abundance of one single taxa.

Even though we identify DSi as a factor controlling bSi and *Pseudo-nitzchia* sp. *cf. delicatissima,* our experimental design precludes discrimination between the role of DSi by itself and the role of its interaction with iron, particularly considering that previous iron addition experiments have shown that Fe levels are important in the promotion of *Pseudo-nitzschia* blooms in coastal waters (Hutchins et al., 1998).

One characteristic of *Pseudo-nitzschia* is its ability to produce DA. The level of cellular DA in the *Pseudo-nitzschia* community was particularly low in + Fe + Si experiments (Fig. 11c), supporting the generalized concept that DA is produced under nutrient (Davidson et al., 2012) and/or Si stress (Fehling et al., 2004; Pan et al., 1998; Pan et al., 1996). The generation of high specific levels of allelopathic substances in some diatom taxa (e.g. DA in *Pseudo-nitzschia*) could be a way to compensate for the vulnerability to grazing associated with lower diatom community silicification in low DSi environments. Our observations suggest that low and constant specific cellular DA concentration in *Pseudo-nitzschia* spp. are associated with high *Pseudo-nitzschia* abundance and high

concentrations of bSi (i.e. + Fe + Si treatment), which agrees with the suggestion that DA production varies inversely with *Pseudo-nitzschia* growth rates (Maldonado et al., 2002). Our results imply that the specific DA cellular content of *Pseudo-nitzschia* could reach a maximum at the western boundary of PAIS (particularly negative Si* waters) due a reduced allochthonous Si supply. This hypothesis needs to be tested in the future given the detrimental impact of DA in ecosystems.

PAIS is expected to have longitudinal gradients in the fluxes of iron and DSi to surface water due the mixing between oceanic water (west) with continental water (east). Eastward increases of DSi and dFe fluxes likely results in neither Fe or Si -stress near the continental sources. Along the E-W salinity gradient, however, the dFe and DSi relief may be uncoupled. for example, when continental subsidies are sufficient to relieve iron stress, but insufficient to relieve DSi stress. In the later conditions of higher new productivity together with high DSi stress, *Pseudo-nitzschia* cells could be particularly toxic. Consistent with this last hypothesis, high levels of DA in mussels have been only reported on the western side of the archipelago (Pizarro et al., 2017) in regions of low continental DSi supply (Torres et al., 2020). A similar rationale has been suggested for the northeast Pacific Ocean (Ribalet et al., 2010). Ribalet et al. (2010) identified the oceanic size of ecotones as optimum condition for blooming of small cell phytoplankton and DA production. We hypothesize that the ratio of bioavailable "continental elements" (e.g. Fe and Si) during the freshening of subantarctic waters (SAASW) could play a role in modifying predator–prey interaction though the degree of toxicity of specific phytoplankton taxońs, as well as by the ability to produce and export bSi.

4.4. The role of environmental dFe and the addition of unchelated dFe.

The internal cycle of iron in surface waters is constituted by a complex matrix of components and processes (Croot & Heller, 2012) and internal fluxes critically determine its bioavailability. In this experiment, the addition of unchelated iron to estuarine water likely caused an acute and transient increase in the concentration of bioavailable iron, follows by the formations of colloids which become rapidly aggregated (Nowostawska et al., 2008) and removed from the dissolved pool. Indeed, ca. 80 % of added Fe did not remain in the < 0.45 μm size fraction. Based on our colloidal iron measurements (0.02–0.45 μm size fraction) we expect that dFe (<0.45 μm) increase relative to controls were allocated in both colloidal fraction and ligand-bound Fe complexes, where extension of the latter depends upon ligand availability. The G1-control, like all other experimental groups controls, showed low levels of nitrate drawdown compared to Fe-enriched treatments (i.e. G1 + Fe and G1 + Fe + Si). However, the dFe concentration in the G1-control was high (12 nM at t = 3) and similar or larger than those measured in Fe-enriched treatments at t = 3, suggesting that the ligand pool in this experimental group (G1) was close to being saturated for dFe, however this initial ligand-Fe complex pool was not entirely available to produce obviously "iron-replete conditions" for macronutrient drawdown, confirming that dFe pool is a poor indicator of what is bioavailable for phytoplankton assimilation (Gobler et al., 2002). Since additions of readily bioavailable iron can eventually trigger luxury iron storage (Cohen et al., 2018; Lampe et al., 2018) or faster iron assimilation in Fe-depleted diatoms compare to Fe-replete diatoms (Chen & Wang, 2008), the increase of nitrate drawdown in Fe-enriched treatments could be attribute to both an initial pulse of unchelated iron (forcing a rapid assimilation and storage of iron) and/or to an enhanced lability of newly formed ligand bond Fe complexes and colloids. Certainly, there are some evidence that phytoplankton can take up Fe derived from colloids and from ligand-bound Fe (Chen & Wang, 2008; Maldonado & Price, 1999; Maldonado et al., 2005) but the latter may largely dependent on the specific phytoplankton and ligand group in question (Blain et al., 2004). Dissolved organic matter of terrestrial origin, a ubiquitous characteristic of estuarine water, contain a wide variety of ligands with varying binding strengths (e.g. Humic acids, HA). Fe^{3+} ions form strong but reversible bonds with hydroxyl and carboxyl groups of HA, allowing the transfer of iron to siderophore-type ligands released by microorganisms for its subsequent uptake (Chen & Wang, 2008) or/and could act as substrate (HA-Fe complexes) to photoreactions that produce highly soluble reduced iron (Croot & Heller, 2012) that can be directly incorporated through microorganism membrane channels. Therefore, is believed that HA play an important role transferring Fe to marine phytoplankton (Batchelli et al., 2010; Chen & Wang, 2008). Our experimental result may indicate that despite a presumably high Fe solubility in coastal waters (forced by marine and continental ligands) the rates of transfer to marine phytoplankton (which may be dependent on a broad range of direct and indirect factors as for example: UV light regimen, characteristics of terrestrial organic matter pool and the availability of siderophore-type ligands) could be insufficient to allow maximum potential productivity levels during a diatom bloom.

In general, the capacity of a unchelated iron addition to intensify macronutrient drawdown (Fig. 5a-b), the positive correlation between the increments in Σ_cdFe and $\Sigma_c$micro-chl a (Fig. 14c) and a nitrate: phosphate drawdown ratio typical of diatom dominated systems (see section 3.2.2.) seem consistent with the hypothesis that pulses of unchelated iron to estuarine water of Patagonia can accelerate diatom new productivity during the study period.

4.5. Integration of the surface waters characteristics in austral spring and iron enrichment experiment results

The negative relationship of nitrate, phosphate and pCO_2 to micro-chl a in surface waters (Table 1) along the latitudinal transect (Fig. 1) indicates that diatoms, which dominate micro-chl a size fraction, were the main driver of surface water new productivity in the study area during September 2017 (austral spring), consistently micro-phytoplankton represent the dominant fraction of phytoplankton community exported from upper layer to subpycnocline waters during the productive season in Patagonian waters (González et al., 2016).

Surface seawater salinity (SSS) and the specific runoff near each station was positively correlated with micro-chl a percentage, but only runoff was negatively correlated to nitrate (Table 1). This pattern may suggest that the drop in nitrate concentration rather than a consequence of freshening per se (i.e. dilution), is a positive response of new productivity to continental solutes (e.g. Fe, Si, Fe + Si).

At the most brackish extreme (i.e. salinity 26) chl a was mostly present in the small size fractions. Our finding of small phytoplankton in the most brackish waters is consistent with previous reports suggesting that brackish waters in southern Patagonia are characterized by small-cell photosynthetic organisms (Díaz-Rosas et al., 2021; Torres et al., 2011a). This surface water salinity minimum located at 52°S (i.e. salinity 26 at St.13) could be associated the influence of glaciated hydrographic basins in southern Patagonia (e.g. Serrano River basin and Estero las Montañas). Although we did not assess any optically active constituents, we hypothesize that optically active particles and solutes from continental origin could produce intense light attenuation (e.g. silt-rich brackish waters associated to subglacial discharges and/or CDOM leached out of the periglacial peatlands, as reported for others fjord systems (Mascarenhas et al., 2017; Paredes and Montecino, 2011)) selecting for small-cell photosynthetic organisms (Chisholm, 1992). However, the effect of CDOM on phytoplankton metabolism may be broader than just its effect on PAR attenuation, for example, UV photoreduction of CDOM ligand-Fe complexes (Croot & Heller, 2012) could provide highly soluble reduced iron, which eventually may help phytoplankton to adapt to low PAR environments. Alternatively, the extreme stratification of brackish waters could favor the persistence of small photosynthetic flagellates (due to their ability to swim to locate themselves in a better PAR regime) compared to large diatoms that require turbulence to avoid sedimentation (Kiørboe, 1993).

At the highest salinities (SSS ~ 30; St. 1, 28 and 29) where the lowest

water column stability was expected, the chemical characteristics of surface waters (low in total-chl a particularly in micro-chl a size range, rich in nitrate with moderate levels Si and pCO_2 levels near equilibrium with the atmosphere) were consistent with a pre-bloom condition in a poorly stratified surface layer, as previously reported for Pacific extreme of Strait of Magellan during Austral spring 1989 (Cabrini and Fonda-Umani, 1991; Saggiomo et al., 1994; Saggiomo et al., 2011) and for Concepción Channel (near station 28–29) during austral spring 2009 (Iriarte et al., 2018). Direct measurements of Gross Primary Productivity (GPP) and community respiration (CR) reported by Iriarte et al. (2018) suggest very low levels of "net productivity" (GPP-CR) in surface waters (e.g. 10 μg C l^{-1} d^{-1}) which contrast with the high levels of productivity (Saggiomo et al., 2011) and biomass reported for the fresher easter portion of the Strait of Magellan. We hypothesize that the reduced haline stratification of the upper water column at the western boundary of the archipelago may delay spring diatom productivity due to light limitation but also due to suboptimal levels of bioavailable Fe as our bottle experiments suggest. Nonetheless, the typical negative Si* values (ca. −6) of salty surface waters (>30) are expected to lead to rapid Si stress as diatom development progresses. If an intense diatom proliferation is triggered in these saltier and moderately DSi rich waters (e.g. due a high irradiance in combination with a pulse of iron bioavailability), the onset of Si stress could lead to the activation of physiological adaptation and selection mechanisms to cope with DSi scarcity (e.g. lower Si:NO_3^- diatom uptake ratio and a reduction of silicification). Indeed, the occurrence of physiological adaptation and/or selection mechanisms to Si stress could explain high Si:NO_3^- drawdown ratios (near 1) in + Fe + Si treatments compared to controls and + Fe treatments (where no DSi was added, see section 3.2.2).

Favorable conditions for augmenting micro chl a and bSi standing stocks, and consequently the drawdown of macronutrients during early spring, seem to occur at intermediate salinity levels. These optimal growth conditions are likely linked to the combined effect of reduced turbulent mixing due to haline stratification, and a complementary mix of marine (N and P) and terrestrial nutrients (Si and micronutrients like Fe). However, our experimental results suggest that even in frontal waters with high diatom productivity, a pulse of highly bioavailable sFe (over a relatively high dFe baseline) could accelerate the nitrate uptake likely due to the particularly high biological demand for Fe and reduction of sFe in these high productivity and high pH levels waters.

During early spring, bioavailable Fe and DSi supply from the continent likely allows for maximum rates of new productivity in surface waters. Consistently, field observations suggested that runoff and surface water nitrate were negatively correlated during the study period (Table 1). Conversely, at higher SSS (e.g. SSS > 30 typically associated with nitrate concentration greater than DSi concentration, see Torres et al. (2014)), suboptimal Fe and/or Si supply could favor the growth of thinner/small diatom community (Leynaert et al., 2004; Marchetti & Cassar, 2009), as well as, small-sized non-silicic functional groups. While the former groups likely base its growth on regenerated nutrients and therefore with limited abilities to produce high rates of new productivity (Eppley and Thomas, 1969), higher new productivity levels of thinner/small diatoms may result in low diatom stocks due an efficient control by micrograzing compared to thicker/large diatom with higher Si needs. A Fe-Si colimitation scenario, may be particularly true under low light regime (Falkowski & Raven, 1997; Raven et al., 1999; Strzepek & Price, 2000), in the study area we expect low light regime at western boundary of Patagonian archipelago (well exposed to open ocean and to Westerlies) associated to a deeper turbulent layer caused by the interaction between low haline stratification and higher wind speeds, and signaled by high surface salinity levels. We hypothesize that a Fe-Si-light colimitation dynamic could better explain reports that salty surface waters are often not depleted in nitrate even at the height of the productive season (a time series showing high salinity high nitrate low silicate conditions near Faro San Isidro at Strait of Magellan is shown in Supplementary Material C).

In summary, this first experimental response of phytoplankton communities in southern PAIS waters to Fe and Fe + DSi amendments, identifies both factors (Fe and Fe + DSi) as capable of modulating aspects of spring diatom bloom dynamics (e.g. community composition and abundance, nutrient drawdown rate, biogenic silica production). The intensity of this modulation is likely sensitive to the location and flux of continental water discharge and the oceanographic characteristics that set the fluxes of marine and continental complementary nutrients. It is also likely to be strongly variable temporally (mainly on seasonal basis), depending on the diatom bloom development stage when continental runoff nutrients pulses do occur. It seems evident that timing of Fe (DSi) fertilization pulses should be a key variable to take in account when assessing the effect of iron, DSi or both on coastal waters phytoplankton stocks. Therefore, care must be taken in extrapolating these first experimental results to other periods and places. Certainly, more focused research is required to better understand the role of continental solutes, their geographic and temporal variability in response to climatic events and local watershed-scale variability, in different aspects of spring bloom characteristics and dynamics at Patagonian waters.

4.6. Concluding remarks

1. Optimum conditions for diatom new productivity and diatom stock accumulation take place within the salinity gradient in inner surface waters of Southern Patagonia Archipelago during austral spring 2017.
2. Environmental variability in both macronutrient and CO_2 was driven by micro phytoplankton in early austral spring 2017, although most of chl a was located in smaller size fractions.
3. Nano-diatoms (e.g. *Minidiscus sp*) were abundant, likely constituting a significant fraction of phytoplankton biomass during early austral spring 2017.
4. Nominal 5 nM unchelated Fe-enrichment of estuarine waters (salinity 28–29) of Concepcion Channel (Southern PAIS) enhance nitrate and phosphate drawdown during an experimentally triggered diatom bloom, even when environmental levels of dFe were relatively high.
5. Early spring diatom bloom characteristics in the Patagonia archipelago, mainly caused by increments light regimen, is likely modulated by the bioavailability of iron and DSi.
6. DSi or DSi + Fe stress relief can enhance standing stocks of *Pseudo-nitzschia* and biogenic silicate, but tends to reduce the specific content of domoic acid in *Pseudo-nitzschia*.
7. Rapid iron-forced depletion of macronutrients probably led to early decay of diatom stocks in experiments with low DSi levels (i.e. + Fe treatments).

Declaration of Competing Interest

The authors declare that they have no known competing financial interests or personal relationships that could have appeared to influence the work reported in this paper.

Data availability

Data will be made available on request.

Acknowledgments

We thank the members of the 2017 field Punta Arenas – Madre de Dios campaign. A special thanks to Steve Beldham for his help with the sampling instrumentation. We thank the Toxin Laboratory of the University of Chile for the analysis of domoic acid, Captain and crew of M/B Forrest for its assistance at sea and Osvaldo Artal at IFOP for its help handling data from the CHONOS-Flow platform (http://chonos.ifop.cl/). This research was primarily funded by FONDECYT 1140385,

additional support was granted by IDEAL (FONDAP-IDEAL Grant 15150003), PATSER (ANID R20F0002) Millennium Science Initiative Program -ICN2021_002 and ANID BASAL FB210018 programs.

Appendix A. Supplementary data

Supplementary data to this article can be found online at https://doi.org/10.1016/j.pocean.2023.102982.

References

Ampuero, P., 2007. Efectos del Fe disuelto sobre la productividad primaria y estructura fitoplanctonica en el centro de surgencias de Coquimbo (30°S). *Departamento de Oceanografía*, Tesis licenciado Biología Marina (p. 84). Universidad de Concepción, Concepción.

Arrigo, K.R., Dunbar, R.B., Lizotte, M.P., Robinson, D.H., 2002. Taxon-specific differences in C/P and N/P drawdown for phytoplankton in the Ross Sea. Antarctica. *Geophysical Research Letters* 29.

Assmy, P., Smetacek, V., Montresor, M., Klaas, C., Henjes, J., Strass, V.H., Arrieta, J.M., Bathmann, U., Berg, G.M., Breitbarth, E., Cisewski, B., Friedrichs, L., Fuchs, N., Herndl, G.J., Jansen, S., Krägefsky, S., Latasa, M., Peeken, I., Röttgers, R., Scharek, R., Schüller, S.E., Steigenberger, S., Webb, A., Wolf-Gladrow, D., 2013. Thick-shelled, grazer-protected diatoms decouple ocean carbon and silicon cycles in the iron-limited Antarctic Circumpolar Current. Proc. Natl. Acad. Sci. 110, 20633–20638.

Batchelli, S., Muller, F.L.L., Chang, K.-C., Lee, C.-L., 2010. Evidence for Strong but Dynamic Iron−Humic Colloidal Associations in Humic-Rich Coastal Waters. Environ. Sci. Tech. 44, 8485–8490.

Bianchi, T.S., 2007. Biogeochemistry of Estuaries. Oxford University Press, New York.

Bianchi, T.S., Arndt, S., Austin, W.E.N., Benn, D.I., Bertrand, S., Cui, X., Faust, J.C., Koziorowska-Makuch, K., Moy, C.M., Savage, C., Smeaton, C., Smith, R.W., Syvitski, J., 2020. Fjords as Aquatic Critical Zones (ACZs). Earth Sci. Rev. 203, 103145.

Blain, S., Guieu, C., Claustre, H., Leblanc, K., Moutin, T., Quèguiner, B., Ras, J., Sarthou, G., 2004. Availability of iron and major nutrients for phytoplankton in the northeast Atlantic Ocean. Limnol. Oceanogr. 49, 2095–2104.

Bouman, H.A., Lepère, C., Scanlan, D.J., Ulloa, O., 2012. Phytoplankton community structure in a high-nutrient, low-chlorophyll region of the eastern Pacific Subantarctic region during winter-mixed and summer-stratified conditions. Deep Sea Res. Part I 69, 1–11.

Boyd, P.W., Jickells, T., Law, C.S., Blain, S., Boyle, E.A., Buesseler, K.O., Coale, K.H., Cullen, J.J., de Baar, H.J.W., Follows, M., Harvey, M., Lancelot, C., Levasseur, M., Owens, N.P.J., Pollard, R., Rivkin, R.B., Sarmiento, J., Schoemann, V., Smetacek, V., Takeda, S., Tsuda, A., Turner, S., Watson, A.J., 2007. Mesoscale Iron Enrichment Experiments 1993–2005: Synthesis and Future Directions. Science 315, 612–617.

Boyle, E.A., Edmond, J.M., Sholkovitz, E.R., 1977. The mechanism of iron removal in estuaries. Geochim. Cosmochim. Acta 41, 1313–1324.

Brzezinski, M.A., Pride, C.J., Franck, V.M., Sigman, D.M., Sarmiento, J.L., Matsumoto, K., Gruber, N., Rau, G.H., Coale, K.H., 2002. A switch from $Si(OH)_4$ to NO_3^- depletion in the glacial Southern Ocean. Geophys. Res. Lett. 29, 5-1-5-4.

Cabrini, M., Fonda-Umani, S., 1991. Phytoplankton populations in the Strait of Magellan. Bolletino di Oceanologia Teorica ed Applicata 9, 137–144.

Calbet, A., Landry, M.R., 2004. Phytoplankton growth, microzooplankton grazing, and carbon cycling in marine systems. Limnol. Oceanogr. 49, 51–57.

Caron, D.A., Alexander, H., Allen, A.E., Archibald, J.M., Armbrust, E.V., Bachy, C., Bell, C.J., Bharti, A., Dyhrman, S.T., Guida, S.M., Heidelberg, K.B., Kaye, J.Z., Metzner, J., Smith, S.R., Worden, A.Z., 2017. Probing the evolution, ecology and physiology of marine protists using transcriptomics. Nat. Rev. Microbiol. 15, 6–20.

Chen, M., Wang, W.X., 2008. Accelerated uptake by phytoplankton of iron bound to humic acids. Aquat. Biol. 3, 155–166.

Chen, J.L., Wilson, C.R., Tapley, B.D., Blankenship, D.D., Ivins, E.R., 2007. Patagonia Icefield melting observed by Gravity Recovery and Climate Experiment (GRACE). Geophys. Res. Lett. 34.

Chisholm, S.W., 1992. Phytoplankton Size. In: Falkowski, P.G., Woodhead, A.D., Vivirito, K. (Eds.), Primary Productivity and Biogeochemical Cycles in the Sea. Springer, US, Boston, MA, pp. 213–237.

Cohen, N.R., Mann, E., Stemple, B., Moreno, C.M., Rauschenberg, S., Jacquot, J.E., Sunda, W.G., Twining, B.S., Marchetti, A., 2018. Iron storage capacities and associated ferritin gene expression among marine diatoms. Limnol. Oceanogr. 63, 1677–1691.

Croot, P., Heller, M., 2012. The Importance of Kinetics and Redox in the Biogeochemical Cycling of Iron in the Surface Ocean. Front. Microbiol. 3.

Cutter, G., Casciotti, K., Croot, P.L., Geibert, W., Haimbürger, L.-E., Lohan, M.C., Planquette, H., van de Flierdt, T., 2017. Sampling and Sample-handeling Protocols for GEOTRACES Cruises. (p. 178).

Davidson, K., Gowen, R.J., Tett, P., Bresnan, E., Harrison, P.J., McKinney, A., Milligan, S., Mills, D.K., Silke, J., Crooks, A.-M., 2012. Harmful algal blooms: How strong is the evidence that nutrient ratios and forms influence their occurrence? Estuar. Coast. Shelf Sci. 115, 399–413.

Dávila, P.M., Figueroa, D., Müller, E., 2002. Freshwater input into the coastal ocean and its relation with the salinity distribution off austral Chile (35–55°S). Cont. Shelf Res. 22, 521–534.

de Baar, H.J.W., de Jong, J.T.M., Nolting, R.F., Timmermans, K.R., van Leeuwe, M.A., Bathmann, U., Rutgers van der Loeff, M., Sildam, J., 1999. Low dissolved Fe and the absence of diatom blooms in remote Pacific waters of the Southern Ocean. Mar. Chem. 66, 1–34.

de Baar, H.J.W., Boyd, P.W., Coale, K.H., Landry, M.R., Tsuda, A., Assmy, P., Bakker, D. C.E., Bozec, Y., Barber, R.T., Brzezinski, M.A., Buesseler, K.O., Boyé, M., Croot, P.L., Gervais, F., Gorbunov, M.Y., Harrison, P.J., Hiscock, W.T., Laan, P., Lancelot, C., Law, C.S., Levasseur, M., Marchetti, A., Millero, F.J., Nishioka, J., Nojiri, Y., van Oijen, T., Riebesell, U., Rijkenberg, M.J.A., Saito, H., Takeda, S., Timmermans, K.R., Veldhuis, M.J.W., Waite, A.M., Wong, C.-S., 2005. Synthesis of iron fertilization experiments: From the Iron Age in the Age of Enlightenment. J. Geophys. Res. Oceans 110.

DeMaster, D.J., 2002. The accumulation and cycling of biogenic silica in the Southern Ocean: revisiting the marine silica budget. Deep Sea Res. Part II 49, 3155–3167.

Díaz-Rosas, F., Alves-de-Souza, C., Alarcón, E., Menschel, E., González, H.E., Torres, R., von Dassow, P., 2021. Abundances and morphotypes of the coccolithophore Emiliania huxleyi in southern Patagonia compared to neighboring oceans and northern-hemisphere fjords. Biogeosciences Discuss. 2021, 1–34.

Dickson, A.G., Millero, F.J., 1987. A comparison of the equilibrium constants for the dissociation of carbonic acid in seawater media. Deep-Sea Res. 34, 1733–1743.

DOE, 1994. Handbook of methods for the analysis of the various parameters of the carbon dioxide system in sea water; version 2.1. In A.G. Dickson, C. Goyet (Eds.), *ORNL/CDIAC-74* (p. 187): U. S. Department of Energy.

Egge, J.K., Aksnes, D.L., 1992. Silicate as regulating nutrient in phytoplankton competition. Mar. Ecol. Prog. Ser. 83, 281–289.

Eppley, R.W., Thomas, W.H., 1969. Comparison of half-saturation constants for growth and nitrate uptake of marine phytoplankton. J. Phycol. 5, 375–379.

Falkowski, P.G., Raven, J.A., 1997. Aquatic photosynthesis. Blackwell Science.

Fehling, J., Green, D.H., Davidson, K., Bolch, C.J., Bates, S.S., 2004. Domoic acid production by Pseufo-Nitzschia seriata (Bacillariophyceae) in scottish waters. J. Phycol. 40, 622–630.

Finkel, Z.V., Beardall, J., Flynn, K.J., Quigg, A., Rees, T.A.V., Raven, J.A., 2010. Phytoplankton in a changing world: cell size and elemental stoichiometry. J. Plankton Res. 32, 119–137.

Forsch, K.O., Hahn-Woernle, L., Sherrell, R.M., Roccanova, V.J., Bu, K., Burdige, D., Vernet, M., Barbeau, K.A., 2021. Seasonal dispersal of fjord meltwaters as an important source of iron and manganese to coastal Antarctic phytoplankton. Biogeosciences 18, 6349–6375.

Franck, V.M., Bruland, K.W., Hutchins, D.A., Brzezinski, M.A., 2003. Iron and zinc effects on silicic acid and nitrate uptake kinetics in three high-nutrient, low-chlorophyll (HNLC) regions. Mar. Ecol. Prog. Ser. 252, 15–33.

Franck, M.V., Brzezinski, M.A., Coale, K.H., Nelson, D.M., 2000. Iron and silicic acid concentrations regulate Si uptake north and south of the Polar Frontal Zone in the Pacific Sector of the Southern Ocean. Deep Sea Res. Part II 47, 3315–3338.

Fujii, M., Ito, H., Rose, A.L., Waite, T.D., Omura, T., 2008. Transformation dynamics and reactivity of dissolved and colloidal iron in coastal waters. Mar. Chem. 110, 165–175.

Glasser, N.F., Harrison, S., Jansson, K.N., Anderson, K., Cowley, A., 2011. Global sea-level contribution from the Patagonian Icefields since the Little Ice Age maximum. Nature Geosci 4, 303–307.

Gobler, C.J., Donat, J.R., Consolvo, J.A., Sañudo-Wilhelmy, S.A., 2002. Physicochemical speciation of iron during coastal algal blooms. Mar. Chem. 77, 71–89.

González, H.E., Graeve, M., Kattner, G., Silva, N., Castro, L., Iriarte, J.L., Osmán, L., Daneri, G., Vargas, C.A., 2016. Carbon flow through the pelagic food web in southern Chilean Patagonia: relevance of Euphausia vallentini as a key species. Mar. Ecol. Prog. Ser. 557, 91–110.

Grasshoff, K., Kremling, K., Ehrhardt, 1999. Methods of Seawater Analysis. WILEY-VCH.

Grønning, J., Kiørboe, T., 2020. Diatom defence: Grazer induction and cost of shell-thickening. Funct. Ecol. 34, 1790–1801.

Haraldsson, C., Anderson, L.G., Hassellöv, M., Hulth, S., Olsson, K., 1997. Rapid, high-precision potentiometric titration of alkalinity in ocean and sediment pore waters. Deep Sea Res., Part I 44, 2031–2044.

Hasle, G.R., Lange, C.B., Syvertsen, E.E., 1996. A review ofPseudo-nitzschia, with special reference to the Skagerrak, North Atlantic, and adjacent waters. Helgoländer Meeresuntersuchungen 50, 131–175.

Hawkings, J.R., Skidmore, M.L., Wadham, J.L., Priscu, J.C., Morton, P.L., Hatton, J.E., Gardner, C.B., Kohler, T.J., Stibal, M., Bagshaw, E.A., Steigmeyer, A., Barker, J., Dore, J.E., Lyons, W.B., Tranter, M., Spencer, R.G., null, N., 2020. Enhanced trace element mobilization by Earth's ice sheets. Proc. Nat. Acad. Sci. 117, 31648–31659.

Hopwood, M.J., Connelly, D.P., Arendt, K.E., Juul-Pedersen, T., Stinchcombe, M.C., Meire, L., Esposito, M., Krishna, R., 2016. Seasonal Changes in Fe along a Glaciated Greenlandic Fjord. *Frontiers*. Earth Sci. 4.

Hopwood, M.J., Carroll, D., Höfer, J., Achterberg, E.P., Meire, L., Le Moigne, F.A.C., Bach, L.T., Eich, C., Sutherland, D.A., González, H.E., 2019. Highly variable iron content modulates iceberg-ocean fertilisation and potential carbon export. Nat. Commun. 10, 5261.

Hutchins, D.A., Bruland, K.W., 1998. Iron-limited diatom growth and Si: N uptake ratios in a coastal upwelling regime. Nature 393, 561–564.

Hutchins, D.A., DiTullio, G.R., Zhang, Y., Bruland, K.W., 1998. An iron limitation mosaic in the California upwelling regime. Limnol. Oceanogr. 43, 1037–1054.

Hutchins, D.A., Sedwick, P.N., DiTullio, G.R., Boyd, P.W., Quéguiner, B., Griffiths, F.B., Crossley, C., 2001. Control of phytoplankton growth by iron and silicic acid availability in the subantarctic Southern Ocean: Experimental results from the SAZ Project. J. Geophys. Res. 106, 2156–2202.

Iriarte, J.L., Kusch, A., Osses, J., Ruiz, M., Iriarte, J.L., 2001. Phytoplankton biomass in the sub-Antarctic area of the Straits of Magellan (53°S), Chile during spring-summer 1997/1998. Polar Biol. 24, 154–162.
Iriarte, J.L., Cuevas, L.A., Cornejo, F., Silva, N., González, H.E., Castro, L., Montero, P., Vargas, C.A., Daneri, G., 2018. Low spring primary production and microplankton carbon biomass in Sub-Antarctic Patagonian channels and fjords (50–53°S). Arct. Antarct. Alp. Res. 50, e1525186.
Kanna, N., Sugiyama, S., Fukamachi, Y., Nomura, D., Nishioka, J., 2020. Iron Supply by Subglacial Discharge Into a Fjord Near the Front of a Marine-Terminating Glacier in Northwestern Greenland. Global Biogeochem. Cycles 34.
Kemp, A.E.S., Pike, J., Pearce, R.B., Lange, C.B., 2000. The "Fall dump" — a new perspective on the role of a "shade flora" in the annual cycle of diatom production and export flux. Deep Sea Res. Part II 47, 2129–2154.
Kiørboe, T., 1993. Turbulence, Phytoplankton Cell Size, and the Structure of Pelagic Food Webs. In: Blaxter, J.H.S., Southward, A.J. (Eds.), Advances in Marine Biology, Vol. 29. Academic Press, pp. 1–72.
Kuma, K., Nishioka, J., Matsunaga, K., 1996. Controls on iron(III) hydroxide solubility in seawater: The influence of pH and natural organic chelators. Limnol. Oceanogr. 41, 396–407.
Kuma, K., Katsumoto, A., Nishioka, J., Matsunaga, K., 1998. Size-fractionated Iron Concentrations and Fe(III) Hydroxide Solubilities in Various Coastal Waters. Estuar. Coast. Shelf Sci. 47, 275–283.
Kunde, K., Wyatt, N., González-Santana, D., Tagliabue, A., Mahaffey, C., Lohan, M., 2019. Iron distribution in the subtropical North Atlantic: The pivotal role of colloidal iron. Global Biogeochem. Cycles 33, 1532–1547.
Lampe, R.H., Mann, E.L., Cohen, N.R., Till, C.P., Thamatrakoln, K., Brzezinski, M.A., Bruland, K.W., Twining, B.S., Marchetti, A., 2018. Different iron storage strategies among bloom-forming diatoms. Proc. Natl. Acad. Sci. 115.
Lewis, W.M., 1976. Surface/Volume Ratio: Implications for Phytoplankton Morphology. Science 192, 885–887.
Lewis, E., Wallace, D., 1998. Program developed for CO2 system calculations. (p. 21). Oak Ridge: Carbon Dioxide Information Analysis Center.
Leynaert, A., Bucciarelli, E., Claquin, P., Dugdale, R., Martin-Jézéquel, V., Pondaven, P., Ragueneau, O., 2004. Effect of iron deficiency on diatom cell size and silicic acid uptake kinetics. Limnol. Oceanogr. 49, 1134–1143.
Liu, H., Chen, M., Zhu, F., Harrison, P.J., 2016. Effect of Diatom Silica Content on Copepod Grazing, Growth and Reproduction. *Frontiers in Marine*. Science 3.
Liu, X., Millero, F.J., 2002. The solubility of iron in seawater. Mar. Chem. 77, 43–54.
Logan, B.E., Passow, U., Alldredge, A.L., Grossartt, H.-P., Simont, M., 1995. Rapid formation and sedimentation of large aggregates is predictable from coagulation rates (half-lives) of transparent exopolymer particles (TEP). Deep Sea Res. Part II 42, 203–214.
López-Rivera, A., Suarez-Isla, B.A., Eilers, P., Beaudry, C., Hall, S., Amandi, M., Furey, A., James, K., 2005. Improved high-performance liquid chromatographic method for the determination of domoic acid and analogues in shellfish: Effect of pH. Anal. Bioanal. Chem. 381, 1540–1545.
Luebert, F., Pliscoff, P., 2006. *Sinopsis bioclimática y vegetacional de Chile*. Santiago de Chile: Editorial Universitaria.
Lürling, M., 2021. Grazing resistance in phytoplankton. Hydrobiologia 848, 237–249.
Maldonado, M., Hughes, M., Rue, E., Wells, M., 2002. The effect of Fe and Cu on growth and domoic acid production by Pseudo-nitzschia multiseries and Pseudo-nitzschia australis. Limnol. Oceanogr. 47, 515–526.
Maldonado, M., Price, N., 1999. Utilization of iron bound to strong organic ligands by plankton communities in the subarctic Pacific Ocean. Deep Sea Res. Part II 46, 2447–2473.
Maldonado, M.T., Strzepek, R.F., Sander, S., Boyd, P.W., 2005. Acquisition of iron bound to strong organic complexes, with different Fe binding groups and photochemical reactivities, by plankton communities in Fe-limited subantarctic waters. Global Biogeochem. Cycles 19.
Marchetti, A., Cassar, N., 2009. Diatom elemental and morphological changes in response to iron limitation: a brief review with potential paleoceanographic applications. Geobiology 7, 419–431.
Marchetti, A., Parker, M.S., Moccia, L.P., Lin, E.O., Arrieta, A.L., Ribalet, F., Murphy, M. E.P., Maldonado, M.T., Armbrust, E.V., 2009. Ferritin is used for iron storage in bloom-forming marine pennate diatoms. Nature 457, 467–470.
Marchetti, A., Varela, D.E., Lance, V.P., Lance, V.P., Palmucci, M., Giordano, M., Virginia Armbrust, E., 2010. Iron and silicic acid effects on phytoplankton productivity, diversity, and chemical composition in the central equatorial Pacific Ocean. Limnol. Oceanogr. 55, 11–29.
Martin, P., van der Loeff, M.R., Cassar, N., Vandromme, P., d'Ovidio, F., Stemmann, L., Rengarajan, R., Soares, M., González, H.E., Ebersbach, F., Lampitt, R.S., Sanders, R., Barnett, B.A., Smetacek, V., Naqvi, S.W.A., 2013. Iron fertilization enhanced net community production but not downward particle flux during the Southern Ocean iron fertilization experiment LOHAFEX. Global Biogeochem. Cycles 27, 871–881.
Martin, J.H., Fitzwater, S.E., 1988. Iron deficiency limits phytoplankton growth in the north-east Pacific subarctic. Nature 331, 341–343.
Martin-Jézéquel, V., Hildebrand, M., Brzezinski, M.A., 2000. Silicon metabolism in diatoms: implications for growth. J. Phycol. 36, 821–840.
Mascarenhas, V.J., Voß, D., Wollschlaeger, J., Zielinski, O., 2017. Fjord light regime: Bio-optical variability, absorption budget, and hyperspectral light availability in Sognefjord and Trondheimsfjord, Norway. J. Geophys. Res. Oceans 122, 3828–3847.
Medlin, L.K., Kaczmarska, I., 2004. Evolution of the diatoms: V. Morphological and cytological support for the major clades and a taxonomic revision. Phycologia 43, 245–270.
Mehrbach, C., Culberson, C.H., Hawley, J.E., Pytkowicz, R.N., 1973. Measurement of the apparent dissociation constants of carbonic acid in seawater at atmospheric pressure. Limnol. Oceanogr. 18, 897–907.
Menden-Deuer, S., Lawrence, C., Franzè, G., 2018. Herbivorous protist growth and grazing rates at in situ and artificially elevated temperatures during an Arctic phytoplankton spring bloom. PeerJ 6, e5264.
Mopper, K., zhou, J., Sri Ramana, K., passow, U., dam, H.G., Drapeau, D.T., 1995. The role of surface-active carbohydrates in the flocculation of a diatom bloom in a mesocosm. Deep Sea Res. Part II 42, 47–73.
Naz, T., Burhan, Z., Munir, S., Siddiqui, P.J.A., 2013. Biovolume and biomass of common diatom species from the coastal waters of Karachi. Pakistan. *Pak. J. Bot* 45, 325–328.
Nishioka, J., Takeda, S., Wong, C.S., Johnson, W.K., 2001. Size-fractionated iron concentrations in the northeast Pacific Ocean: distribution of soluble and small colloidal iron. Mar. Chem. 74, 157–179.
Nowostawska, U., Kim, J., Hunter, K., 2008. Aggregation of riverine colloidal iron in estuaries: A new kinetic study using stopped-flow mixing. Mar. Chem. 110, 205–210.
Olenina, I., Hajdu, S., Edler, L., Andersson, A., Wasmund, N., Busch, S., Göbel, J., Gromisz, S., Huseby, S., Huttunen, M., Jaanus, A., Kokkonen, P., Jurgensone, I., Niemkiewicz, E., 2006. Biovolumes and size-classes of phytoplankton in the Baltic Sea. HELCOM Balt. Sea Environ. Proc., 106.
Öztürk, M., Steinnes, E., Sakshaug, E., 2002. Iron Speciation in the Trondheim Fjord from the Perspective of Iron Limitation for Phytoplankton. Estuar. Coast. Shelf Sci. 55, 197–212.
Palma, S., Silva, N., 2004. Distribution of siphonophores, chaetognaths, euphausiids and oceanographic conditions in the fjords and channels of southern Chile. Deep Sea Res. Part II 51, 513–535.
Pan, Y., Rao, D.V.S., Mann, K.H., Li, W.K.W., Harrison, W.G., 1996. Effects of silicate limitation on production of domoic acid, a neurotoxin, by the diatom Pseudo-nitzschia multiseries. II. Continuous culture studies. Mar. Ecol. Prog. Ser. 131, 235–243.
Pan, Y., Bates, S.S., Cembella, A.D., 1998. Environmental stress and domoic acid production by Pseudo-nitzschia: a physiological perspective. Nat. Toxins 6, 127–135.
Paredes, A., Montecino, V., 2011. Size diversity as an expression of phytoplankton community structure and the identification of its patterns on the scale of fjords and channels. Cont. Shelf Res. 31, 272–281.
Pizarro, G., Frangópulos, M., Krock, B., Zamora, C., Pacheco, H., Alarcón, C., Toro, C., Pinto, M., Torres, R., Guzmán , L., 2017. Watch out for ASP in the Chilean Subantarctic region. In L.A.O. Proença, G.M. Hallegraeff (Eds.), *Marine and Fresh-Water Harmful Algae. Proceedings of the 17th International Conference on Harmful Algae* (pp. 30-33). Florianópolis, Brazil: International Society for the Study of Harmful Algae.
Pryer, H., Wadham, J.L., Hawkings, J.R., Robinson, L.F., Hendry, K.R., Marshall, M., Yates, C., Hatton, J.E., 2019. Glacial cover affects nutrient fluxes from rivers in Chilean Patagonia. *Goldshmidt*. Barcelona.
Pryer, H., Hawkins, J., Wadham, J.L., Robinson, L.F., Hendry, K.R., Hatton, J.E., Gill Olivas, B., Kellerman, A., Marshall, M., Daneri, G., Bertrand, S., Haussermann, V., Brooker, R., 2020. Glacial cover affect silicon and iron exports from rivers. Global Biogeochem. Cycles 34, e2020GB006611.
Ragueneau, O., Savoye, N., Del Amo, Y., Cotten, J., Tardiveau, B., Leynaert, A., 2005. A new method for the measurement of biogenic silica in suspended matter of coastal waters: Using Si: Al ratios to correct for the mineral interference. Cont. Shelf Res. 25, 697–710.
Ragueneau, O., Tréguer, P., 1994. Determination of biogenic silica in coastal waters: applicability and limits of the alkaline digestion method. Mar. Chem. 45, 43–51.
Ragueneau, O., Tréguer, P., Leynaert, A., Anderson, R.F., Brzezinski, M.A., DeMaster, D. J., Dugdale, R.C., Dymond, J., Fischer, G., François, R., Heinze, C., Maier-Reimer, E., Martin-Jézéquel, V., Nelson, D.M., Quéguiner, B., 2000. A review of the Si cycle in the modern ocean: recent progress and missing gaps in the application of biogenic opal as a paleoproductivity proxy. Global Planet. Change 26, 317–365.
Raiswell, R., Canfield, R.E., 2012. The Iron Biogeochemical Cycle Past and Present. Geochemical Perspective 1, 1–220.
Raiswell, R., Tranter, M., Benning, L.G., Siegert, M., De'ath, R., Huybrechts, P., Payne, T., 2006. Contributions from glacially derived sediment to the global iron (oxyhydr) oxide cycle: Implications for iron delivery to the oceans. Geochim. Cosmochim. Acta 70, 2765–2780.
Raiswell, R., Hawkings, J., Elsenousy, A., Death, R., Tranter, M., Wadham, J., 2018. Iron in Glacial Systems: Speciation, Reactivity, Freezing Behavior, and Alteration During Transport. Front. Earth Sci. 6, 1–17.
Raven, J.A., Evans, M.C.W., Korb, R.E., 1999. The role of trace metals in photosynthetic electron transport in O2-evolving organisms. Photosynth. Res. 60, 111–150.
Ribalet, F., Marchetti, A., Hubbard, K.A., Brown, K., Durkin, C.A., Morales, R., Robert, M., Swalwell, J.E., Tortell, P.D., Armbrust, E.V., 2010. Unveiling a phytoplankton hotspot at a narrow boundary between coastal and offshore waters. Proc. Natl. Acad. Sci. 107, 16571–16576.
Rivera, P., Koch, P., 1984. Contributions to the diatom flora of Chile II. In: Mann, D.G. (Ed.), Proceedings of the Seventh International Diatom Symposium, Philadelphia, August 22–27, 1982. Koeltz Science Publishers, Koenigstein, pp. 279–298.
Ryderheim, F., Grønning, J., Kiørboe, T., 2022. Thicker shells reduce copepod grazing on diatoms. Limnol. Oceanogr. Lett. 7, 435–442.
Saggiomo, V., Goffart, A., Carrada, G.C., Hecq, J.H., 1994. Spatial patterns of phytoplanktonic pigments and primary production in a semi-enclosed periantarctic ecosystem: the Strait of Magellan. J. Mar. Syst. 5, 119–142.
Saggiomo, V., Santarpia, I., Saggiomo, M., Margiotta, F., Mangoni, O., 2011. Primary production processes and photosynthetic performance of a unique periantarctic ecosystem: The Strait of Magellan. Polar Biol. 34, 1255–1267.

Saito, H., Ota, T., Suzuki, K., Nishioka, J., Tsuda, A., 2006. Role of heterotrophic dinoflagellate Gyrodinium sp. in the fate of an iron induced diatom bloom. Geophys. Res. Lett. 33.
Sarmiento, J.L., Gruber, N., Brzezinski, M.A., Dunne, J.P., 2004. High-latitude controls of thermocline nutrients and low latitude biological productivity. Nature 427, 56–60.
Schoffman, H., Lis, H., Shaked, Y., Keren, N., 2016. Iron-Nutrient Interactions within Phytoplankton. *Frontiers*. Plant Sci. 7.
Schroth, A.W., Crusius, J., Hoyer, I., Campbell, R., 2014. Estuarine removal of glacial iron and implications for iron fluxes to the ocean. Geophys. Res. Lett. 41, 3951–3958.
Sedwick, P.N., Blain, S., Quéguiner, B., Griffiths, F.B., Fiala, M., Bucciarelli, E., Denis, M., 2002. Resource limitation of phytoplankton growth in the Crozet Basin, Subantarctic Southern Ocean. Deep Sea Res. Part II 49, 3327–3349.
Seo, H., Kim, G., Kim, T., Kim, I., Ra, K., Jeong, H., 2022. Trace elements (Fe, Mn Co, Cu, Cd, and Ni) in the East Sea (Japan Sea): Distributions, boundary inputs, and scavenging processes. Mar. Chem. 239, 104070.
Sholkovitz, E.R., 1976. Flocculation of dissolved organic and inorganic matter during the mixing of river water and seawater. Geochim. Cosmochim. Acta 40, 831–845.
Sholkovitz, E.R., Boyle, E.A., Price, N.B., 1978. The removal of dissolved humic acids and iron during estuarine mixing. Earth Planet. Sci. Lett. 40, 130–136.
Smetacek, V., 1998. Biological oceanography: Diatoms and the silicate factor. Nature 391, 224–225.
Smetacek, V., Klaas, C., Strass, V.H., Assmy, P., Montresor, M., Cisewski, B., Savoye, N., Webb, A., d/'Ovidio, F., Arrieta, J.M., Bathmann, U., Bellerby, R., Berg, G.M., Croot, P., Gonzalez, S., Henjes, J., Herndl, G.J., Hoffmann, L.J., Leach, H., Losch, M., Mills, M.M., Neill, C., Peeken, I., Rottgers, R., Sachs, O., Sauter, E., Schmidt, M.M., Schwarz, J., Terbruggen, A., Wolf-Gladrow, D., 2012. Deep carbon export from a Southern Ocean iron-fertilized diatom bloom. Nature 487, 313–319.
Smith, R.B., Evans, J.P., 2007. Orographic precipitation and water vapor fractionation over the Southern Andes. J. Hydrometeorol. 8, 3–19.
Steinberg, D.K., Landry, M.R., 2017. Zooplankton and the Ocean Carbon Cycle. Ann. Rev. Mar. Sci. 9, 413–444.
Strickland, J.D.H., Parsons, T.R., (Eds.), 1968. A practical handbook of seawater analysis.
Strzepek, R.F., Harrison, P.J., 2004. Photosynthetic architecture differs in coastal and oceanic diatoms. Nature 431, 689.
Strzepek, R.F., Price, N.M., 2000. Influence of irradiance and temperature on the iron content of the marine diatom Thalassiosira weissflogii (Bacillariophyceae). Mar. Ecol. Prog. Ser. 206, 107–117.
Sunda, W.G., Huntsman, S.A., 2011. Interactive effects of light and temperature on iron limitation in a marine diatom: Implications for marine productivity and carbon cycling. Limnol. Oceanogr. 56, 1475–1488.
Tagliabue, A., Bowie, A.R., DeVries, T., Ellwood, M.J., Landing, W.M., Milne, A., Ohnemus, D.C., Twining, B.S., Boyd, P.W., 2019. The interplay between regeneration and scavenging fluxes drives ocean iron cycling. Nat. Commun. 10, 4960.
Takeda, S., 1998. Influence of iron availability on nutrient consumption ratio of diatoms in oceanic waters. Nature 393, 774–777.
Tillmann, U., Hesse, K.-J., Tillmann, A., 1999. Large-scale parasitic infection of diatoms in the Northfrisian Wadden Sea. J. Sea Res. 42, 255–261.
Torres, R., Ampuero, P., 2009. Strong CO_2 outgassing from high nutrient low chlorophyll coastal waters off central Chile (30°S): The role of dissolved iron. Estuar. Coast. Shelf Sci. 83, 126–132.
Torres, R., Turner, D., Silva, N., Ruttlant, J., 1999. High short-term variability of CO2 fluxes during an upwelling event off the Chilean coast at 30S. Deep Sea Res., Part I 46, 1161–1179.
Torres, R., Frangopulos, M., Hamamé, M., Montecino, V., Maureira, C., Pizarro, G., Reid, B., Valle-Levinson, A., Luis Blanco, J., 2011a. Nitrate to silicate ratio variability and the composition of micro-phytoplankton blooms in the inner-fjord of Seno Ballena (Strait of Magellan, 54°S). Cont. Shelf Res. 31, 244–253.
Torres, R., Pantoja, S., Harada, N., González, H.E., Daneri, G., Frangopulos, M., Rutllant, J.A., Duarte, C.M., Rúiz-Halpern, S., Mayol, E., Fukasawa, M., 2011b. Air-sea CO2 fluxes along the coast of Chile: From CO2 outgassing in central northern upwelling waters to CO2 uptake in southern Patagonian fjords. J. Geophys. Res. 116, C09006.
Torres, R., Silva, N., Reid, B., Frangopulos, M., 2014. Silicic acid enrichment of subantarctic surface water from continental inputs along the Patagonian archipelago interior sea (41–56°S). Prog. Oceanogr. 129, Part A, 50–61.
Torres, R., Reid, B., Frangópulos, M., Alarcón, E., Márquez, M., Häussermann, V., Försterra, G., Pizarro, G., Iriarte, J.L., González, H.E., 2020. Freshwater runoff effects on the production of biogenic silicate and chlorophyll-a in western Patagonia archipelago (50–51°S). Estuar. Coast. Shelf Sci. 241, 106597.
Utermohl, H., 1958. Zur Ver vollkommung der quantitativen phytoplankton-methodik., Mitteilung Internationale Vereinigung Fuer Theoretische unde. Amgewandte Limnologie 9, 39 p.
von der Heyden, B.P., Roychoudhury, A.N., 2015. A review of colloidal iron partitioning and distribution in the open ocean. Mar. Chem. 177, 9–19.
Willis, M.J., Melkonian, A.K., Pritchard, M.E., Ramage, J.M., 2012. Ice loss rates at the Northern Patagonian Icefield derived using a decade of satellite remote sensing. Remote Sens. Environ. 117, 184–198.
Yeats, P.A., Bewers, J.M., 1976. Trace metals in the waters of the Saguenay fjord. Can. J. Earth Sci. 13, 1319–1327.
Zhang, S., Liu, H., Ke, Y., Li, B., 2017. Effect of the silica content of diatoms on protozoan grazing. Front. Mar. Sci. 4.